Chapter-5

Experimental Study and Results

5.1 Proximate, Ultimate and GCV Analysis

5.1.1 Introduction

Coal, according to the United Nation Economic Commission for Europe (UN-ECE), contains more organics (> 50) than inorganic (Ward and Suárez-Ruiz, 2008a).The general characteristics of coal include the analysis of coal's organic, inorganic, and energy content, known as its GCV. The ultimate analysis determines the presence of essential elements which includes carbon, hydrogen, nitrogen, oxygen, and sulfur. Their quantitative information is vital, and elements like carbon and hydrogen are helpful in the determination of rank as well as in the characterization of coal for coking, gasification, and liquefaction (hydrogenation) processes (Khare and Dell'Amico, 2013). Nitrogen and sulfur are both potential pollutants(Chen et al., 2007). Coal, as a fossil energy is a good source of energy. For the optimization of energy consumption, the characterization of coal is essential. The detailed assessment of coal from five different mines is elaborated below.

Name of Mines	Table 5.1 Proximate, ultimate analysis, and GCV of coal in the Singrauli										GCV (kcal/kg)
	Samples	Proximate Analysis				Ultimate analysis					
		Moisture	VM	Ash	FC	C	N	H	O	S	
Bina	PCA 5	5.00	28.90	22.80	43.30	53.66	0.42	3.14	19.53	0.45	4151
	PCA 4	4.00	28.00	28.00	40.00	49.03	1.26	4.14	16.37	1.20	3701
	PCA 3	5.50	23.50	29.00	42.00	55.00	2.89	3.99	18.62	0.50	3998
	PCA 2	5.00	29.00	21.00	45.00	58.04	1.58	4.67	13.83	0.89	4964
	PCA 1	3.90	31.60	16.80	47.70	60.02	0.94	4.52	17.17	0.55	5250
	Average	**4.60**	**28.20**	**23.50**	**43.60**	**55.10**	**1.41**	**4.10**	**17.10**	**0.71**	**4412.80**
Kakri	PCB5	6.13	29.75	20.25	43.88	65.01	0.91	4.80	14.74	0.55	5022
	PCB4	4.00	32.60	17.00	46.70	53.90	0.76	4.32	17.80	0.78	5250
	PCB3	6.10	27.00	26.30	40.60	54.29	0.76	4.27	17.80	0.78	4533
	PCB2	4.00	26.80	8.00	61.20	64.60	0.86	4.74	18.62	0.49	6262
	PCB1	6.80	28.80	12.00	52.40	70.01	2.15	4.14	17.33	0.40	5854
	Average	**5.30**	**29.80**	**18.30**	**50.60**	**61.70**	**1.20**	**4.40**	**18.40**	**0.66**	**5438.80**
Krisnashila	PCC5	5.00	28.60	15.00	51.40	62.81	1.76	3.88	16.33	**0.22**	**5630**
	PCC4	6.00	30.00	15.00	49.00	60.84	1.71	3.84	23.84	0.33	5521
	PCC3	7.00	30.00	20.10	42.9	55.37	1.17	4.86	21.08	0.92	4830
	PCC2	6.10	28.00	23.00	42.90	51.18	0.72	3.40	29.31	0.39	4920
	PCC1	4.50	31.10	20.00	44.40	54.46	1.42	2.82	28.36	0.70	5280
	Average	**5.70**	**29.50**	**18.60**	**46.10**	**56.93**	**1.30**	**3.70**	**23.70**	**0.51**	**5236.20**
Dudhichua	PCD9	5.30	26.60	40.00	30.60	53.19	1.06	4.60	15.53	0.54	4050
	PCD8	6.20	21.90	36.20	35.70	51.42	0.96	4.05	15.78	0.60	4333
	PCD7	5.40	25.90	39.60	31.40	49.15	1.69	3.59	23.87	0.70	4021
	PCD6	6.50	28.50	35.10	32.90	48.26	1.73	3.66	16.47	0.48	4179
	PCD5	4.80	30.00	37.90	30.70	49.59	1.36	4.81	18.55	0.70	4243
	PCD4	4.70	32.90	22.10	43.20	49.97	2.25	4.33	13.38	0.67	5778
	PCD3	5.40	31.10	33.20	34.00	51.10	0.84	3.49	18.03	0.54	4707
	PCD2	4.80	28.30	31.60	38.20	51.27	1.99	3.69	18.33	0.58	4827
	PCD1	4.10	30.20	21.70	46.10	60.74	1.96	4.28	14.57	0.45	5673
	Average	**5.20**	**26.60**	**33.00**	**35.80**	**51.60**	**1.50**	**4.10**	**17.10**	**0.58**	**4645.60**
Jayant	PCM 8	8.00	30.00	32.00	30.00	33.71	1.32	3.78	13.11	0.92	3243
	PCM 7	6.00	32.80	10.00	51.20	54.84	1.34	4.49	12.53	0.08	5954
	PCM 6	5.60	32.00	18.00	44.40	66.21	1.72	4.81	17.17	0.55	5902
	PCM 5	8.00	28.00	33.50	30.50	31.66	1.19	3.80	21.08	0.92	3295
	PCM 4	10.00	25.00	23.00	42.00	33.49	1.18	2.90	17.40	0.73	3693
	PCM 3	6.00	31.00	11.00	52.00	62.54	1.94	4.74	18.33	0.60	5901
	PCM 2	7.00	22.00	11.20	54.55	59.80	2.97	5.70	13.11	0.75	6274
	PCM 1	6.40	31.60	17.00	45.00	51.54	1.90	3.60	17.68	0.61	6056
	Average	**7.10**	**28.90**	**19.46**	**43.71**	**49.22**	**1.60**	**4.20**	**16.30**	**0.64**	**5039.70**

5.2 Thermogravimetric (TGA) Analysis

5.2.1 Introduction: The TGA technique is based on mass loss at variable temperatures due to heating at a constant rate. In this methodology, a given sample is heated via a computer-controlled heating process. The graph obtained between temperature and mass loss is called the thermo-gravimetric (TG) curve, and the derivative of the TGA curve is called the differential thermo-gravimetric (DTG) curve. The TGA technique is widely used to analyze the various parameters (chemical and physical) of coal properties. The TGA and DTG techniques are useful for studying various chemical processes during coal combustion, including the oxidation and pyrolysis of aliphatic and aromatic compounds. It is a far more efficient technique for estimating coal parameters in thermal industries than the traditional ASTM/DIN method. For understanding the chemical reactivity pattern and quality control purposes, TGA and DTA are also helpful. Coal is susceptible to spontaneous combustion during transport. It depends on the nature and type of coal constituents in which moisture and VM play a prime role (Janković et al., 2020). The use of coal for energy generation has numerous technical disadvantages during combustion. Increasing its efficiency and related environmental problems are prime concerns. Many issues are related to the transportation and storage of coal. Self-heated coal is the prime concern (Mohalik et al., 2018).

5.2.2 Theory of TGA

Thermo-gravimetric analysis (TGA) has been carried to understand the non-isothermal combustion behavior of coal and to estimate other kinetic parameters. The standard experimental protocol has been followed for this study of thermo-gravimetric analysis. Numerous characteristic combustion parameters such as initial temperature for the pyrolysis (Ti), the initial temperature of the fast pyrolysis (Tm), the maximum

temperature of pyrolysis (Tmax), and pyrolysis ending temperature of (Tf) under oxy-fuel environments can be directly obtained from the TGA and DTG curves (Aich et al., 2020; Dwivedi et al., 2022b; Mohalik et al., 2017; Mohalik et al., 2009a).

5.2.3 Kinetics analysis of TGA Data

An analyzer (TGA-50 M/s Shimadzu by Asia Pacific Ltd.) has been used to understand the kinetics of the pyrolysis of coal samples. The rate of reaction can be calculated with the Arrhenius equation, which is given below (Aich et al., 2020; Dwivedi et al., 2019; Dwivedi et al., 2022b; Ken et al., 2018; Kumar and Nandi, 2021a; Marangwanda et al., 2021):

$$\frac{d\alpha}{dt} = Ae^{\frac{-E}{RT}}f(\alpha) \quad \textbf{(i)}$$

Where α refer to degree of conversion, t is time, T is reaction temperature, A is frequency factor, E denotes activation energy, R is for universal gas constant (8.314 J/ (mol.K)),and f(α)is called the function for reaction. The value of(α);estimated from the TGA data from the equation given below:

$$\alpha = \frac{m_0 - m_T}{m_0 - m_f} \quad \textbf{(ii)}$$

Where, m_0 represents initial mass of the coal sample, m_T remaining mass of coal sample at temperature T, and m_f refers to the final remaining mass of the coal sample after end of the combustion.

The function f(α) expressed by equation $f(\alpha)=(1-\alpha)^n$, where n denotes the order of the reaction as a function of temperature. Equation (iii) can be used to calculate the constant heating rate ($\beta = \frac{dT}{dt}$). The Coats-Redfern (CR) equation can be used to estimate kinetic parameters such as activation energy of coal combustion (Aich et al.,

2020; Dwivedi et al., 2019; Dwivedi et al., 2022b; Kumar and Nandi, 2021a)using data of TGA and given below:

$$\ln\left(\beta\frac{d\alpha}{dT}\right) = \ln\left[A\left(f(\alpha)\right)\right] - \frac{E_a}{RT} \quad \textbf{(iii)}$$

The slope of the graph between$\ln\left(\frac{-\ln(1-\alpha)}{T^2}\right)$, and $\frac{1}{T}$ using the equation (iii) gives the value of activation energy for the coal samples.

5.2.4 Analysis of TGA Profile

The loss temperature was recorded under different pyrolysis circumstances for the TGA analysis. The TGA graphs of six different properties of coal have been plotted and given in Figure5.1 (a), (b), (c), (d), (e), and (f)**.** In the current study, coal 1, coal 2, coal 3, and coal 4 have comparatively low ash, while coal 5 and 6 have high ash yields.

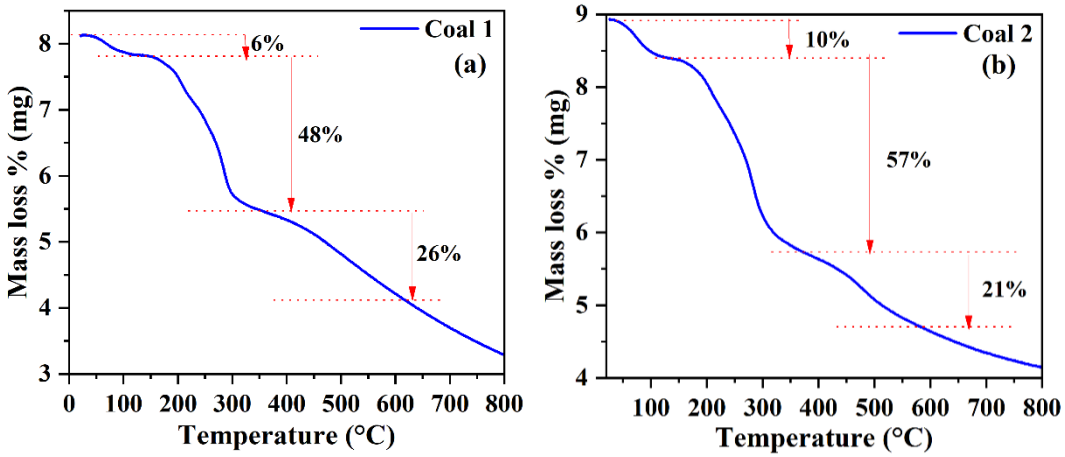

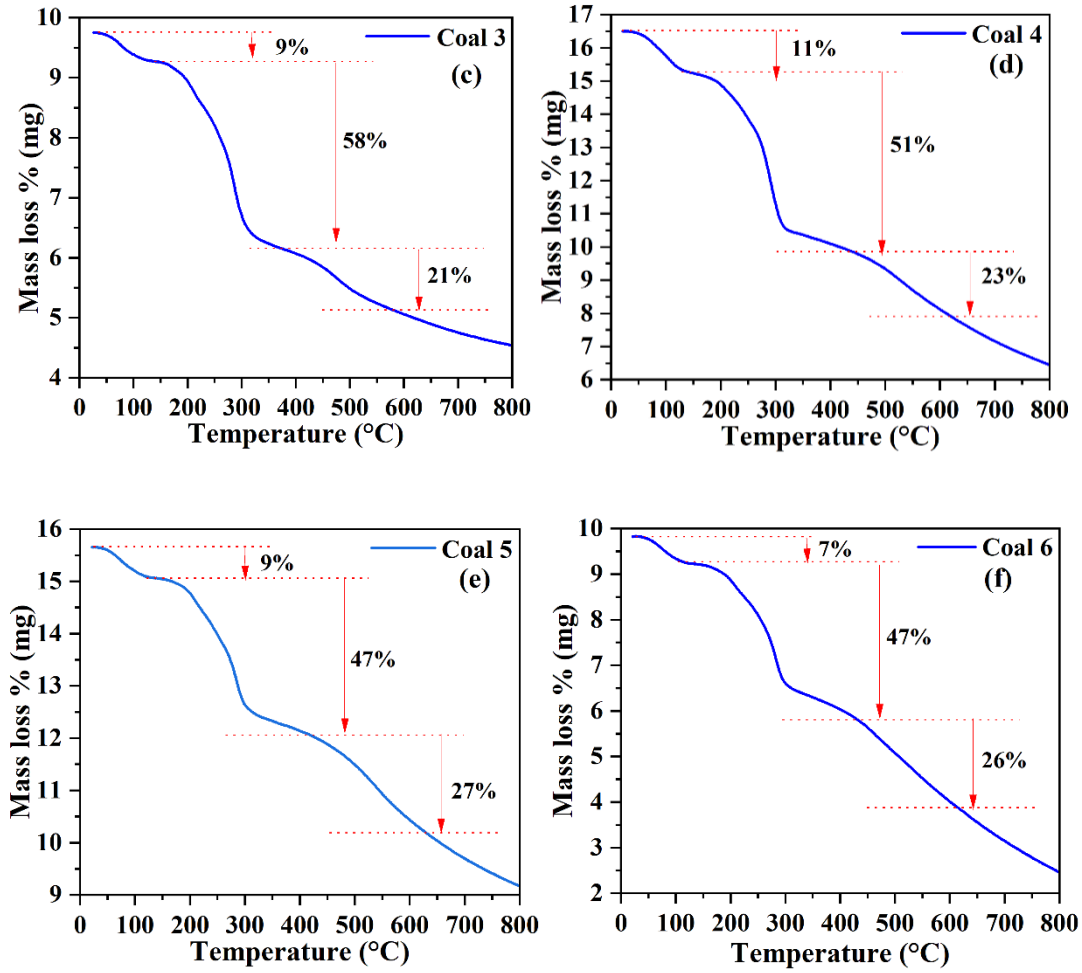

Figure 5.1. TGA profile of six different coal samples as **(a)** Coal 1, **(b)** coal 2, **(c)** coal 3, **(d)** coal 4, **(e)** coal 5, and **(f)** coal 6, respectively.

The pyrolysis of the coal samples depended on their chemical constituents and reactivity. Endothermic reactions occur due to water losses in the form of vapors, and major exothermic reactions can be easily understood in three stages. In the first stage of pyrolysis of coal samples, the water vapors and moisture have been removed from the coal surfaces, and during this stage, some depolymerization conversion also occurs. Moisture or water vapor discharge occurs between the temperatures of 110 °C and 350 °C during pyrolysis. The secondary stage of coal combustion takes place between 350 °Cto650 °C. In the second stage of the coal pyrolysis, the volatile matter is reduced, followed by the burning of the heterogeneous organic constituents in the coal matrixes. Specifically, two or three exothermic peaks may be observed in the

second phase of the coal pyrolysis related to their combustion. In the second stage of the reaction, there is approximately 60%–80% weight loss in the coal sample. The third stage occurs between the 650°C-1000°C temperature range. The exothermic peak recorded during the third stage occurs due to the decomposition and breakdown of the mineral constituents present in the sample (Behera et al., 2020; Dwivedi et al., 2018; Nguyen et al., 2020; Saikia et al., 2009; Song et al., 2016).

Table 5.2. Burning profile parameters and combustion rate of different coal samples										**GCV (kcal/kg)**
No. of Samples	**T_C (°C)**	**T_i (°C)**	**T_{max}(°C)**		**T_n (°C)**	**T_f (°C)**	**Mass loss (%) in (T_i - T_n) zone**	**$DTG_{max\ 1}$ (mass%/min)**	**$DTG_{max\ 1}$ (mass%/min)**	
			T_1	**T_2**						
Coal 1	75	140	283	489	630	790	48	3.38	0.75	6056
Coal 2	81	150	280	481	620	792	57	3.10	0.78	6274
Coal 3	78	148	286	471	640	785	58	4.33	0.89	6262
Coal 4	98	155	291	520	631	790	51	7.89	1.39	5250
Coal 5	74	151	286	540	640	798	47	4.13	1.37	3295
Coal 6	99	153	291	521	640	795	47	4.80	1.31	3243

Where, T_c = maximum temperature for the moisture loss, T_i = Initial temperature for the pyrolysis, T_m= Initial temperature of the fast pyrolysis, T_{max}= maximum temperature of pyrolysis, and T_f = ending temperature of pyrolysis.

The TGA graph shows that water vapor and moisture loss occur between 70 and 110 °C. During this process, weight loss is approximately 6–11% of coal samples. Furthermore, a slight increase in mass has been detected in the 120-170 °C temperature range, which could be due to oxygen absorption on the coal surface. After 170 °C, a sharp fall in mass with temperature was observed in all the coal samples, showing the initiation of the coal combustion process. Such a sharp fall and weight loss might be due to the burning of volatiles and organic materials in the 170 °C to 350 °C temperature range during this decomposition. Weight loss in coal

samples is 47–58% in this range.

Further, the TGA curve also moves to the higher temperature range with an increase in temperature. Above 350 °C, at 350–667 °C, decomposition corresponding to different mineral phases and weight loss percentage is approximately 21–27% for coal samples. Furthermore, the above 650 °C discharge of solid residue occurred in the pyrolysis of coal samples. Hence, the major devolatilization phase of the coal sample occurs in the range of 200–670 °C, also known as the active pyrolysis zone, as represented in Figure 5.1. In an active zone, the pyrolysis process of coal intensifies, and volatile matter comes out very quickly and forms a solid residue (charcoal/fly ash). After 670 °C, temperature devolatilization does not happen; hence, no further weight loss occurs in coal pyrolysis. This zone is called the passive zone. In this zone, the final solid residue is formed as ash. It has been observed that the final residue increases in weight with an increase in the initial weight of the coal because of ash associated with Permian coal. However, the pyrolysis behavior is approximately the same for all the samples. Yuan et al. (2021), Kumar and Nandi, (2021a, b), and Marangwanda et al.(2021) also obtained a similar TGA patterns.

5.2.5 Analysis of DTG Profile

The differential thermogravimetric (DTG) curve gives information about the peak at which a maximum rate of weight loss observed in the coal sample or peaks correspond to the point of highest gradient in the TGA curve. The point corresponding to the minimum inflection in the DTG curve is known as DTG_{max} and corresponds to a temperature known as T_{max}(Ken et al., 2018; Marangwanda et al., 2021). DTG_{max} can be represented as:

$$DTG_{max} = \left|\left(\frac{d\alpha}{dt}\right)_{max}\right| \text{.....(iv)}$$

In Figure 5.2, (a), (b), (c), (d), (e), and (f) represent the different DTG profiles of the coal samples taken for analysis in an oxygen environment. Various parameters related to the DTG curve, such as T_c (maximum temperature for the moisture loss), Ti (initial temperature for the pyrolysis), T_m (initial temperature of the fast pyrolysis), T_{max} (maximum temperature of pyrolysis), Tf (ending temperature of pyrolysis) and DTG_{max} have been found and presented in Table 5.2**.** From the DTG curve, it can be observed that coal pyrolysis shows three peaks, first in the 70–110°C range. The second peak is in the 140-350°C range, and the third peak is in the 350-650°C temperature range. The maximum loss in weight obtained in the lower temperature range of 140–350 °C in all the coal samples corresponds to devolatilization and volatile oxidation or partial combustion of organic matter present in the coal sample. In the second stage, there is also a small peak in the range of 420–530 °C due to the combustion of mineral matter present in coal. The combustion mass recorded for all samples at 650–800 °C shows little to no change. Various researchers (Kumar and Nandi, 2021a, b; Yuan et al., 2021; Marangwanda et al., 2021) also reported a similar DTG plot pattern with different types of samples.

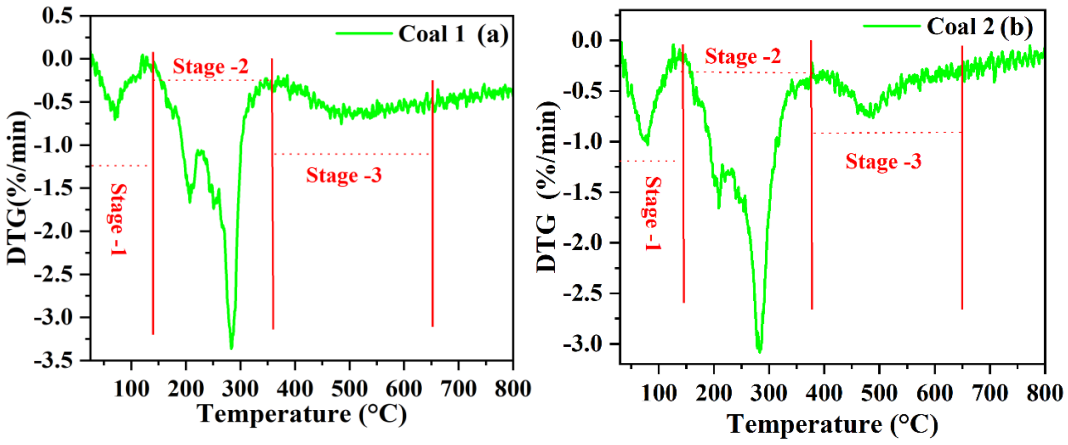

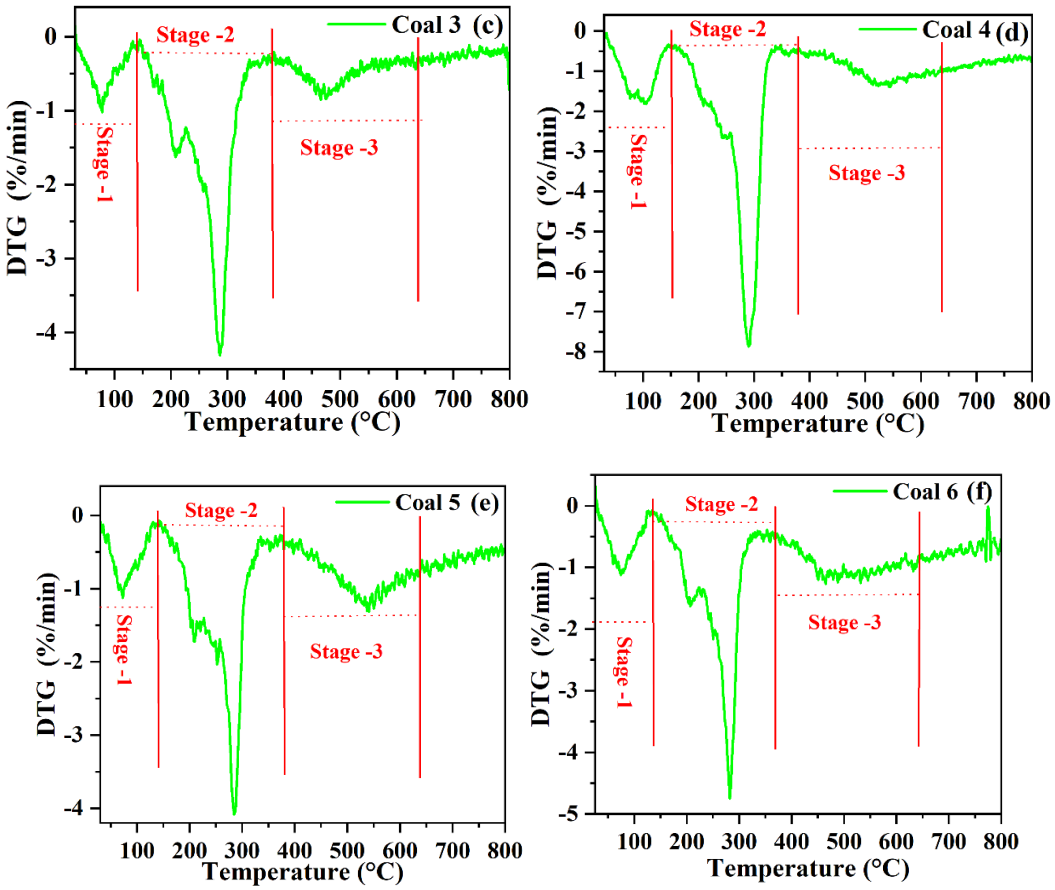

Figure 5.2. DTG profile of different coal samples (a-f) as **(a)** Coal 1, **(b)** Coal 2, **(c)** Coal 3, **(d)** Coal 4,**(e)** Coal 5,and **(f)** Coal 6 respectively.

5.2.6 Analysis of activation energy (E_a)

Analysis of activation energy (E_a) for different coal samples has been carried out using the Coats-Redfern method**.** TGA data has been used for the estimation of activation energy using the equation (iii) (Aich et al., 2020; Dwivedi et al., 2018; Dwivedi et al., 2019; Dwivedi et al., 2022b; Ken et al., 2018; Kumar and Nandi, 2021a). Hence, the slope of graph between $\ln(\frac{-\ln(1-\alpha)}{T^2})$ and $\frac{1}{T}$plotted using Equation (iii) gives the value of the activation energy and frequency factor for the coal samples, and values are tabulated in Table 5.3**.** From the observations, it can be concluded that activation energy varies from 63–169 kJ/mol for different coal samples. It can also be observed that the conversion degree obtained in the case of all the samples lies in the range of 0.34-0.54 and the mean correlation coefficient (R^2) value lies in the range of

0.965-0.999. These results of activation energy also match with the previous reported work by Dwivedi et al.(2022b) reported activation energy of bituminous coal in the range 34.66–396.52 kJ/mol in another work by Aich et al. (2020) and Dwivedi et al. (2020) reported activation energy of Indian coal is 56.85-86.24 kJ/mol and 46.27 kJ/mol, respectively.

Table 5.3 Estimated value of Conversion degree (α) Activation energy (Eg) and Correlation coefficient (R^2)

No. of Samples	Activation energy(kJ/mol)	Conversion degree (α)	Correlation coefficient (R^2)
Coal 1	63.57	0.53	0.973
Coal 2	74.45	0.50	0.972
Coal 3	79.66	0.52	0.973
Coal 4	122.5	0.53	0.972
Coal 5	126.9	0.34	0.965
Coal 6	169.5	0.45	0.999

5.2.7 Conclusion

Six Permian bituminous coal samples have been studied for combustion characteristics, pyrolysis behavior, and kinetics parameters through TGA and DTG analysis. The present study helps to understand the ignition and combustion performance of high ash and low ash bituminous coal considering the physicochemical constraints. The kinetic parameters were determined using the Arrhenius equation, and activation energies were calculated by using the Coats-Redfern method. Further detailed study of different combustion parameters reveals that the activation energy varies from 63–169 kJ/mol for different coal samples, and, values of activation energies for low-rank coal were found to be high (169.5 kJ/mol). It has been observed that the conversion degree obtained lies in the range of 0.34-0.54, and the mean correlation coefficient (R^2) value lies in the range of 0.965-0.999. This study can be beneficial to understanding the combustion performance of coal and

help us use low-rank coal to upgrade environmental and energy constraints efficiently.

5.3 XRD Mineralogy of Coal

XRD is a non-destructive analytical technique used to collect information about atomic positions, arrangements, and the spacing pattern within the lattice structure. Coal is composed of atoms arranged in a crystalline microstructures (Ali et al., 2022; Gilmore et al., 2019). The crystalline inorganic minerals generated in coal during the pre and post-depositional stages having a well-defined chemical composition. Amorphous materials in coal have an irregular arrangement of atoms, but crystalline materials have a regular arrangement of atoms. The knowledge and identification of minerals present in coal are essential for the effective and better utilization of coal (Cuéllar-Franca and Azapagic, 2015; Lee, 2017)

The XRD pattern of the spectra of four different coals is given in Figure 5.3 (a-d). The peak intensities show fewer variations due to the same source of the material; mineral phase resulting peaks were compared with the database of JCPDS (Joint Committee on Powder Diffraction Standards), which are based on the nature, type, and orientation of crystal structures (McMurdie et al., 1986) . XRD analysis enables us to identify several minerals present in coal. The most intense peak at $2\theta = 26.6°$ corresponds to quartz, indicating that it is a main fraction in the sample. Here, seven Q peaks have been seen with varied positions and intensities, indicating high contents of different forms of quartz (SiO_2) were present in the coal, resulting in a high ash content in the coal. It is worth noting that the quartz peak intensity of the size fraction was significantly higher than that of other identified size fraction, indicating that these quartz in samples were mainly gangue minerals associations in coal. The analyzed XRD diffractogram of coal reveals a significant phases of quartz, kaolinite, gypsum, crystals, followed by muscovite, orthoclase, sulfur, hematite, siderite, pyrite, jarosite, and chlorite. The presence of these mineralogical elements and their atomic arrangement in the crystal lattice influence coal's physical and chemical properties**.**

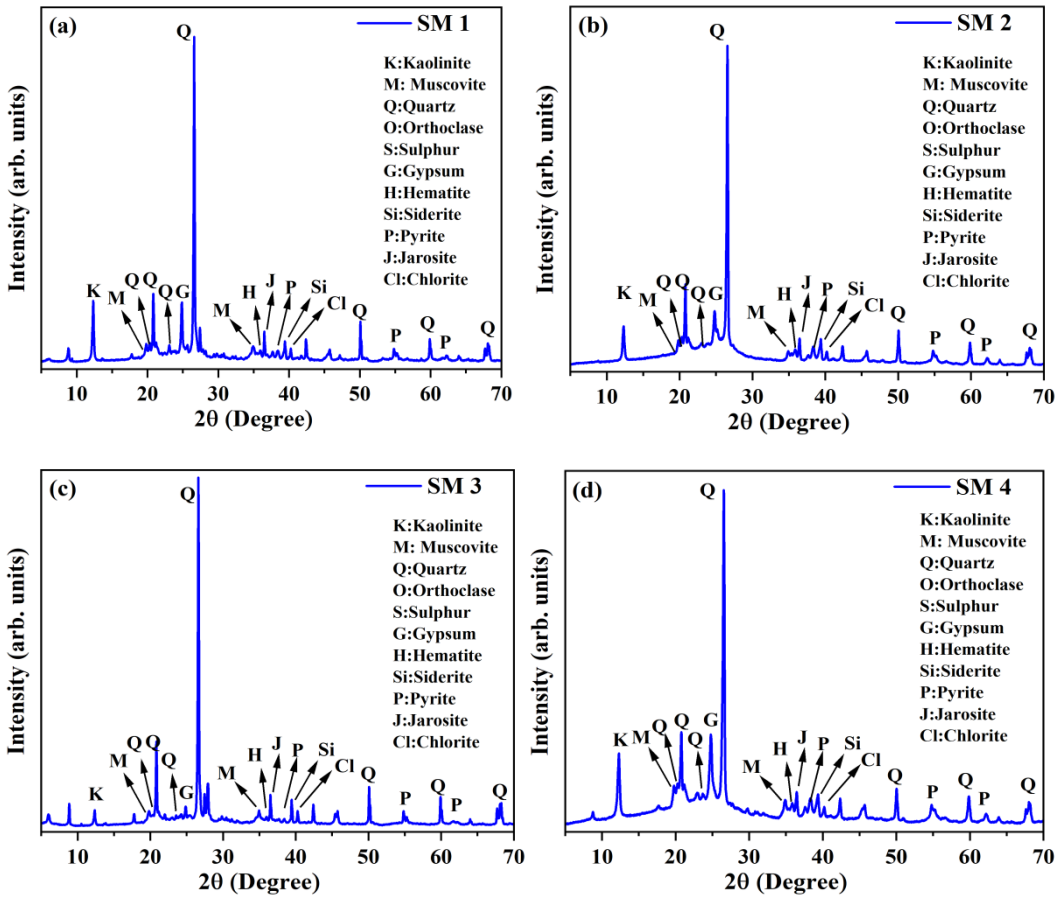

Figure 5.3. Qualitative XRD analysis of coal samples showing the presence of mineral phases (Q: Quartz; K:Kaolinite; M:Muscovite; O:Orthoclase; H: Hematite; Si:Siderite; G: Gypsum; P: Pyrite; S:Sulphur; J:Jarosite; and Cl: Chlorite).

Coal contains a noticeable amount of clay, carbonate, oxide, and sulfide minerals. Dai et al.(2014)reported that detrital fragments form of quartz and kaolinite in the coal; present mainly in fissures, cracks, cleats, and cell fillings in the organic matter, indicating the process of deposition by authigenic precipitation. Kaolinite, a clay mineral, is abundant and occurs as isolated patches filled with quartz or in association with quartz. In coal, quartz is present in two forms: a detrital euhedral form associated with clay such as kaolinite and illite and authigenic quartz and clays linked with organic pores. It often occurs as vermicular aggregates (Dai et al., 2014). It is non-reactive during coal utilization due to its high fusion temperature (around 1800 °C). However, during reactions, high-temperature quartz phases such as

cristobalite and tridymite may be formed (Reifenstein et al., 1999). The coarser quartz fragments may cause abrasion during the grinding and pulverization (Raask, 1985). Kaolinite is associated with K, Na, Mg, and other alkali earth elements. Clay minerals occur in the groundmass as fillings in the fissures, cracks, and cleats in coal macerals. Siderite is the main carbonate mineral in Singrauli coal. Siderite appears as small irregular bodies or patches, fissure fillings, or cavity fillings (Singh et al., 2015b).

The presence of pyrite in coal agrees with the dominance of the deltaic environment during the deposition of coal-bearing Barakar sediments in the basins of the Singrauli Coalfield, as suggested by (Chakraborty and Kumar, 2003) as fissure and crack fillings, the distribution of these minerals in coal depends on the type of plant community, climate, depositional milieu, water conditions (pH and Eh), and the tectonic framework of the basin. Syngenetic pyrite in coal is believed to have resulted primarily through the interaction of dissolved iron and H_2S, the latter being created by bacterial reduction of sulfate ions in the peat mire's reducing environment (Querol et al., 1989; Williams and Keith, 1963). Dai et al.(2012b) reported syngenetic pyrite in coals generated in lacustrine, and other comparable freshwater-dominated environments that did not get any seawater injection (Ward, 2002b). Percolated epithermal or hydrothermal waters, sulfate-rich lake waters, or sulfate-rich groundwater are thought to be involved in pyrite formation in such instances(Dai et al., 2002). Jiang et al.(2016) reported different pyrite forms in Permian coal, including pure nodular pyrite samples indicating different origins: vein-filling (rich in trace elements, probably epigenetic), framboidal (barren, probably syngenetic), and nodular pyrites. Other studies have also shown many variations between pyrite forms in the same coal of the same origin. Pyrite is a sulfide present in Singrauli coal in a minor amount. Both epigenetic and syngenetic conditions favor the pyrite and siderite

formation. The decomposition of pyrite generates iron sulfate (mainly ferrous sulfate, $FeSO_4$ and ferric sulfate, $Fe_2(SO_4)_3$) (Hu et al., 2006),which causes acid drainage problems(Dutta et al., 2020). Jarosite ($KFe_3(SO_4)_2(OH)_6$), most likely derived from pyrite oxidation in Permian coal samples, pyrite (FeS_2) oxidation, may form iron oxides and shows chemical alteration with calcite and it is a prime source of acid mine drainage. Hematite (Fe_2O_3) is a type of iron oxide present in the sample. These are primarily non-reactive and contribute to ash fractions after burning (Ward, 2016a).

5.4 SEM Analysis

SEM has been used to determine the morphological characteristics of materials. SEM/EDS is a powerful technique to determine the elemental composition of minerals. The significant advantage of SEM is that it can examine minerals without destroying morphological and chemical features in the sample. These images (photomicrographs) provide detailed observations of surface and association with the minerals present in coal (Jones et al., 1992). The mineral analysis provides knowledge about the coal matrix, nature, and habits. The main minerals identified in Singrauli coal have been quartz and aluminosilicates. Clay minerals are present abundantly in the sample, especially kaolinite, illite, and montmorillonite. Kaolinite is the most dominant mineral. As seen in the Figure 5.4, the clay mineral present in coal is lamellar and plate-like, sandwiched between the two coal macerals.

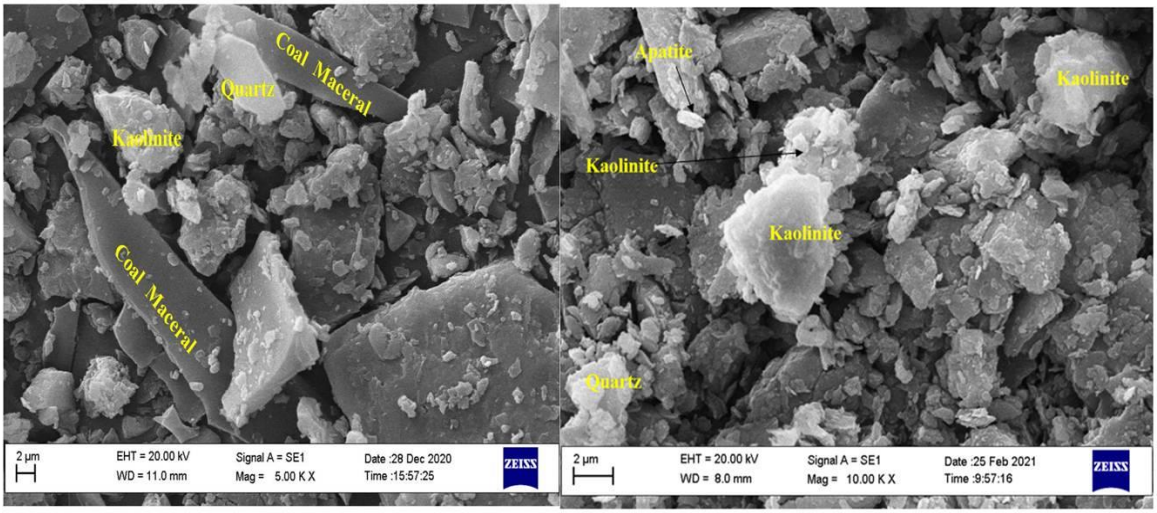

Figure 5.4. SEM image showing the presence of coal macerals along with mineral particles.

In the high-ash Indian Permian coal, massive clay minerals are extensively and non-uniformly present in the sample. Kaolinite is the most abundant clay mineral found. The smaller clay particles were also seen (Figure 5.4)**.** Cell filings also contain clay-containing minerals. The presence of kaolinite in organic cells indicates the authigenic formation process. Well-crystallized kaolinite indicates in situ formation (Ding et al., 2009).The high pH environment favors the growth of authigenic kaolinite in coal by the association of alumina and silica. Tiny particles of quartz have been observed in coal. These smaller particles of quartz are formed by an authigenic process and distributed in macerals (Bhowmick et al., 2017) . Many cracks, fissures, cleats, and veins were also present. Etched pits, layers, some islands, hills, and valleys could also be randomly distributed throughout the SEM photomicrograph. It was inferred that the coal under study contains large proportions of silica, calcium carbonates, dolomite, and some elements such as aluminum, potassium, and sulfur (Singh et al., 2013).

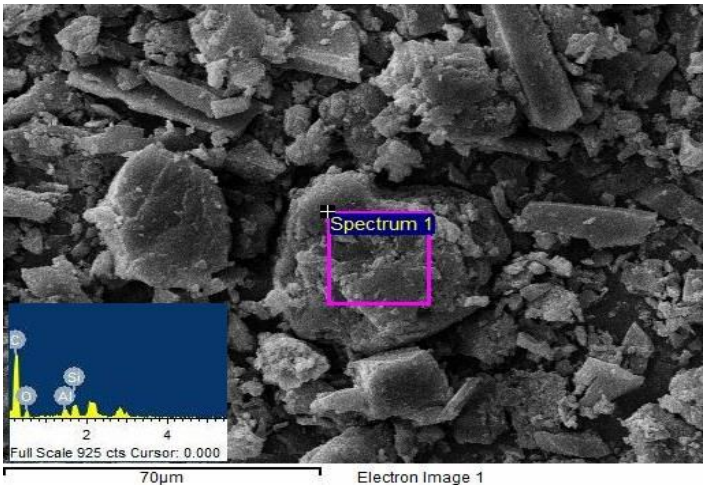

Figure 5.5. Energy-dispersive X-ray spectroscopy (EDX) graph of elements associated with the Indian Permian coal from Singrauli coalfield, India. The survey detected the presence of carbon, oxygen, silicon, and aluminum as significant constituents.

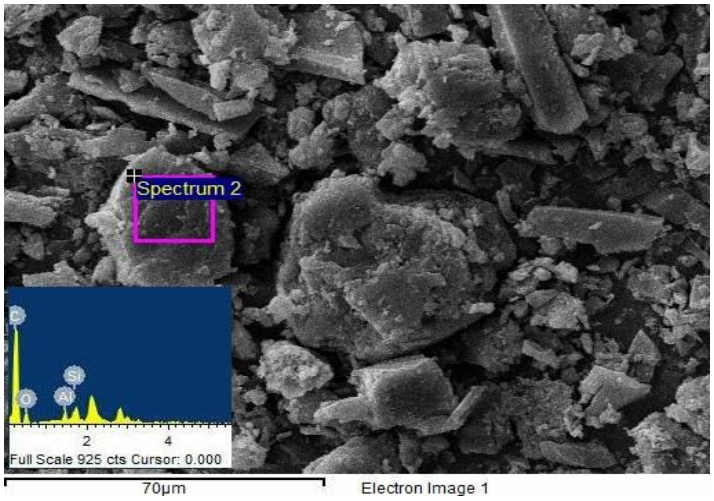

Figure 5.6 Energy-dispersive X-ray spectroscopy (EDX) graph of elements associated with the Indian Permian coal from Singrauli coalfield, India. The survey detected the presence of carbon, oxygen, silicon, and aluminum as significant constituents.

Indian Permian coal is the high-ash and low-grade quality that generates a huge amount of fly ash in thermal power plants. Silica as quartz (SiO_2) is present in crystalline and amorphous forms along with CaO as a common constituent in the fly ash. After combustion, a huge amount of fly ash has been generated, impacting the

local environment directly or indirectly. During boiler operation, fly ash causes slagging and fouling (Jiao et al., 2016).Trace metals present in coal provide challenges for managing and assessing contaminants during beneficiation (Dai et al., 2005). Many workers reported that the potential economic recovery of trace elements present in coal-derived fly ash is controlled by the nature and chemical composition of the terrigenous sediment (Yao et al., 2014) .Therefore, the study of fly ash is essential to know its potential utility.

5.5 FTIR Analysis

5.5.1 Introduction: FTIR spectroscopy has been carried out to decipher the presence of organic (aliphatic and aromatic) and inorganic (silicate, carbonate and hydroxyl) components in the coal sample (Saikia et al., 2007). FTIR works on the phenomenon known as absorption, which occurs at a particular wavenumber due to their specific chemical bonds, intrinsic physicochemical properties of molecules, the occurrence of amorphous organic material, and the presence of clay minerals (Ghosh and Bandopadhyay, 2020).

5.5.2 FTIR characterization of the coals

Figure 5.7 displays the characteristic transmittance peaks for coal samples and reveals the presence of different functional groups (Arenillas et al., 2004). However, for the analysis of these groups, quantitative results can be obtained by considering the peak area as well as the height of peaks. Therefore, for the quantitative analysis, peak area has been calculated using the Gaussian function peak processing method (Solomon and Carangelo, 1982). In the present study, the following different functional groups have been observed in the Permian coal samples.

Table 5.4 Characteristic peaks and respective molecular vibrations

Number of Band	Band Region (cm^{-1})	Functional Group/ Mineral Present
1.	690	C-S, Fe
2.	776-730	Aromatic(-CH) groups
3.	770-794	Quartz, Si-O Symmetric
4.	880-860	Aromatic nucleus (CH), one adjacent H deformation
5.	1032-1070	Si-O Stretching of clay mineral, Si-O-Si asymmetric stretching vibration
6.	1380	Symmetric deformation -CH_2 groups
7.	1435	Bending vibrations of aliphatic ethyl (-CH_2) and methyl-CH_3 groups
8.	1615-1650	Vibrations of aromatic groups (-C=C)
9.	1721-1730	Vibrations of aromatic (carbonyl/carboxyl groups) (-C=O), aliphatic (aldehyde-ketone, acid), (-C=O) groups
10.	2400-2000	Inorganic Carbonyl compounds
11.	2848-2863	Aliphatic CH_3 symmetric stretching vibration
12.	2919-2975	Aliphatic CH_3 and -CH_2 asymmetric stretching vibration
13.	3080-3037	Aromatic nucleus CH stretching vibration
14.	3600-3200	−OH stretching vibration
15.	3625-3700	Illite / Muscovite / Kaolinite

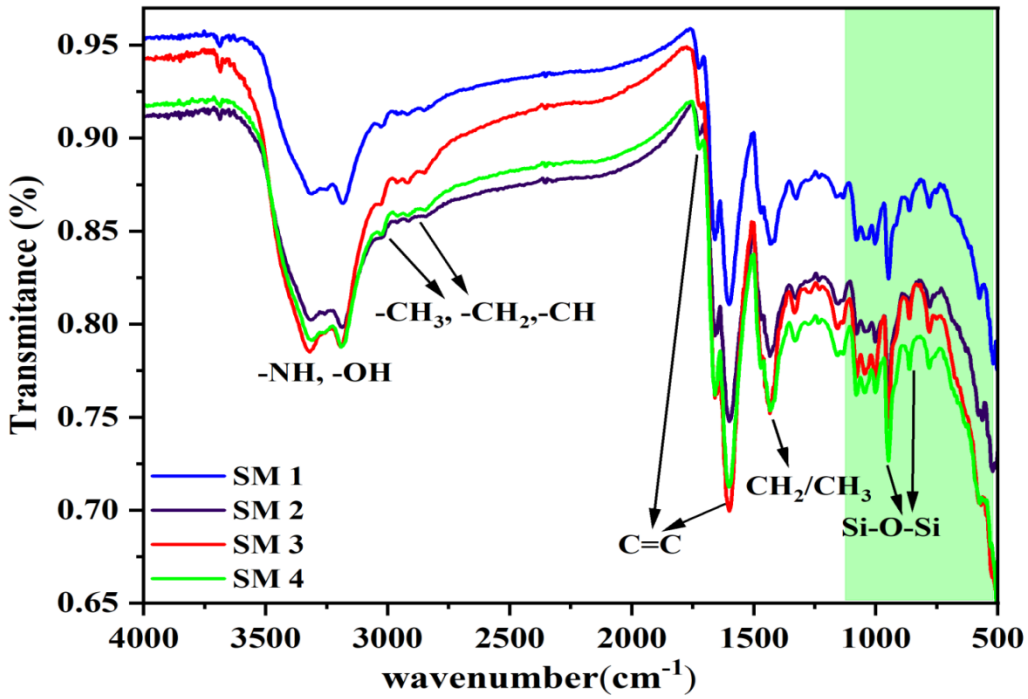

Figure 5.7. FTIR spectra of the different coal samples.

Table 5.5 Peak area of characteristic transmittance peaks of different coal samples

Classification of peak structure	**Aromatic hydrocarbon groups**			**Aliphatic hydrocarbon groups**				**Oxygen containing functional group**		
Peak position (cm^{-1})	**756**	**914**	**1692**	**1327**	**1432**	**2838**	**2911**	**1025**	**1104**	**3309**
Associated functional group	**-CH**	**-CH**	**-C=C**	**-CH (methyl)**	**-CH (methylene and methoxy)**	**-CH (Methyl-CH_2)**	**-CH (Methyl-CH_3)**	**-C-O-H**	**-C=O**	**-OH (hydrogen bonded hydroxyl)**
SM-1	0.06	3.10	6.05	1.38	8.03	0.01	0.04	2.01	1.07	26.8
SM-2	1.63	1.58	9.97	0.78	8.39	0.16	0.13	5.77	4.68	26.1
SM-3	0.58	3.85	11.1	0.37	8.41	0.61	0.54	2.85	1.08	33.2
SM-4	0.65	4.09	7.92	1.76	10.06	0.51	0.31	2.70	2.76	36.9

5.5.3 Aliphatic Hydrocarbon Groups

The estimation of aliphatic hydrocarbon groups is a powerful tool in the quantitative understanding of coal. It is helpful for the identification of long-chain paraffin or olefins present in coal (Dwivedi et al., 2022a).It also indicate the CBM potential of coal seam (Panwar et al., 2017) . The transmittance peaks at 2838 cm^{-1},

and 2911 cm^{-1} correspond to stretching vibrations of -CH_3 of aliphatic groups and symmetric stretch vibrations of methyl (-CH_3) groups. However, the vibrational peaks at 1327 cm^{-1}, and 1432 cm^{-1} correspond to the symmetric vibrations of the aliphatic methoxy groups and asymmetric -CH_3 groups, respectively. The peaks close to 2908 cm^{-1} and 2838 cm^{-1} arise due to alicyclic -CH, -CH_2, and -CH_3 groups. It can also be seen that there is a peak intensity at 2908 cm^{-1} having a greater intensity as compared to the 2838 cm^{-1} peak, which indicates the existence of a long chain of aliphatic groups in these samples. The vibrational peak is located near 1693 cm^{-1} due to carbonyl (C=O) vibrations. These peaks occurred due to vinylic (-C=C), aromatic C=C, stretches, and many other -C=C (aromatic ring/benzene ring) rich organic constituting the functional groups (Ibarra et al., 1996; Smook, 2007; Yue et al., 2021).A small band near 1442 cm^{-1} mainly refers to the -CH_3 asymmetric deformation due to -CH_2 vibrations. These vibrations might be correlated with aromatic (C=C) vibrations and hydrogen-bonded hydroxyl (OH) vibrations.

5.5.4 Aromatic Hydrocarbon Groups

The aromatic structures in the coal samples can be represented by transmittance peaks of 1692 cm^{-1}, 914 cm^{-1}, and 756 cm^{-1}, respectively, given in Table 5.4. The aromatic ring (C=C) can be identified near 1692 cm^{-1}. The vibration between 870 cm^{-1} and 745 cm^{-1} has been attributed to aromatic vibrations (Hu et al., 2014; Saikia et al., 2009; Smook, 2007). The peaks at 3672 cm^{-1},and 3569 cm^{-1} are due to the stretching vibration of the -OH group. A small peak is present at 3041 cm^{-1}indicatesaromatic hydrogen bands and high substitution and condensed behavior. The Carbonyl (C=O) group's vibration peaks are seen near 1693 cm^{-1}. These peaks occurred due to vinylic (-C=C), aromatic C=C, stretches, and many other-C=C (aromatic ring/benzene ring) rich in organics. The peak at 1581 cm^{-1} has been ascribed

either to C=C or due to benzene rings. These functional groups mainly include alcohol, phenol, carbonyl, carboxylic acid, and ether groups that originate in coal due to the decomposition of diverse plant materials. Vibration near 1356 cm^{-1} is due to methyl ($-CH_3$) symmetric deformation. This vibration near 1356 cm^{-1}also corresponds to methyl ($-CH_3$) and ethyl ($-CH_2$) vibrations in cyclic structures. The intensity of 1356 cm^{-1} is less intense than 1442 cm^{-1}. This represents the methylene group as a long aliphatic side chains (Georgakopoulos, 2003; Jaiswal and Pal, 2020; Naktiyok, 2020). The hydrogen-bonded phenolic and alcoholic group vibrations are at 3309 cm^{-1} and transmittance peak near 1025 cm^{-1}, and 1104 cm^{-1}correspond to phenolic C-O-H and carboxylic C=O vibrational band, and they are polar and hydrophilic (Wang et al., 2012).

5.5.5 Oxygen-Containing Functional Groups:

Oxygen is associated with phenolic and alcoholic groups with transmittance peaks near 1025 cm^{-1} and 1104 cm^{-1}, corresponding to phenolic (C-O-H) and carboxylic (–C=O) vibrations. Hydroxyl groups vibration are present in FTIR spectra in the 3600–3200 cm^{-1} range, indicating the presence of hydrogen bonding in structures, and the peak area corresponding to these vibrations is shown in Table 5.9(Wang et al., 2012). The intensities and areas of these peaks are used to quantify carboxylic and phenolic groups that appear in the sample. It can be seen from FTIR, the transmittance peak of the carboxylic acid is at 1108 cm^{-1} and for phenolic -C-OH is at 1025 cm^{-1}. Similarly, the transmittance peak for phenolic-C-O-H is at 1025 cm^{-1}. The trend is similar for all the coals (Yue et al., 2021).

5.5.6 Inorganic Mineral Phases: A broad absorption peak between 3800 cm^{-1}, and 3500 cm^{-1} may indicate-OH stretching vibrations or the presence of inherent moisture in the sample. The vibrations in the 110-500 cm^{-1} correspond to the clay mineral

groups such as quartz, kaolinite, illite, montmorillonite, oligoclase, and feldspar; peak at 1005 cm^{-1} is due to the Si-O-Si stretching vibration (Rawat and Yadav, 2020; Xing et al., 2016). The next peak at 3412 cm^{-1} appears due to -NH vibration. Small vibrations at 690 cm^{-1} indicate the presence of the C-S band. The strong absorption at 530 cm^{-1} attributed to the Si–O bending vibration. Vibration near 530 cm^{-1} shows the existence of ionic sulfates and Si-O-Al phases. A weak absorption at 1166 cm^{-1} of is present in coal samples due presence of quartz, and the band near 690 cm^{-1} might be due to the presence of iron oxide (Fe_2O_3) (Dwivedi et al., 2022a; Kumar and Nandi, 2021b; Rawat and Yadav, 2020; Saikia et al., 2009; Xing et al., 2016).Hence, it can be deduced that mineral matter influences the characteristics and presence of various functional groups in samples.

5.5.7 Conclusion

FTIR spectra of Indian Permian coal samples reveal that they incorporate oxygen-containing, aliphatic, and aromatic functional groups. It has been found that there are a considerable number of hydrophobic functional groups such as (CH, CH_2, and CH_3). Oxygen-containing functional groups such as (C=O) carbonyl or carboxide, (C-O,-OH) alcohol, phenol, and (COO-) carboxyl groups are hydrophilic. The results of Indian Permian coal from Singrauli mines found that the inherent hydrophobicity is high. It also indicates a low degree of ordered microcrystalline units with a low degree of aromatic conformation. The samples have the most significant proportion of oxygenated functional groups, followed by aromatic structures, aliphatic structures, and hydroxyl groups. Results from this study are helpful in the study of molecular structural characteristics of coal and our understanding of properties such as wettability and pore structure.

5.6 XPS Analysis

5.6.1. Introduction: Coal is a complex heterogeneous material with different organic and inorganic (mineral) matters and exhibits a wide range of physical properties derived during coalification. Its inorganic components are referred to as minerals, while its organic components are macerals, deriving from a vegetable source (Dai et al., 2020). Macerals are microscopic organic constituents of coal, possessing distinctive physical and chemical properties, primarily botanical in origin, determined using reflected light and fluorescence microscopy (Teichmüller, 1990) .In addition, coal macerals are characterized according to their texture, structure, and degradation properties (Hower et al., 1996a). The degree of chemical, physical, and biological alterations in the macerals ranges from nearly original tissues to those that have undergone significant change, both before and after their integration into the peat and continuing during the peatification and coalification processes. The Coal metamorphism changes the organic composition and maceral chemistry. Coal petrographic indices describe the macerals, and minerals composition as well as its depositional environment (Jasper et al., 2017).

A wide variety of minerals occur within coal (Finkelman et al., 2019b).Coal has associations with two types of minerals: syngenetic and digenetic (Ward, 2002b). Syngenetic minerals, formed during the peatification process, and digenetic minerals have been introduced, remobilized, or converted from other minerals in the coal at any stage after the initially coal-forming peat was buried or during coalification (Dai and Finkelman, 2018b; Ruppert et al., 1993). When coal is exposed to the surface, different minerals may appear as a consequence of the oxidation of sulfide along with other minerals(van Krevelen, 1982).The abundance and modes of occurrence of minerals, specifically authigenic minerals that developed in situ in the peat mire

during or shortly after the peat development (e.g., framboidalpyrite, nodular siderite, and a number of cell and pore-filling minerals such as quartz, kaolinite, pyrite, and phosphate minerals) (Dai et al., 2016), may provide useful details not only for better understanding the geological setting but also for determining the depositional environment (Finkelman et al., 2019b).According to Dai et al. (2017), the presence of terrigenous-origin minerals such as carbonate and kaolinite indicate depositional settings (Dai et al., 2016). Interaction with fluids that percolated through the coal bed during diagenetic or epigenetic stages may influence mineral chemistry (Dai and Finkelman, 2018b). The arrangement and interactions of macerals and inorganic minerals inside coal components should control the surface properties of coal (Polat et al., 2003).The differences in coal surface chemistry arise due to the oxidation(Bend and Kosloski, 1993), of various maceral groups, and the presence of minerals (Fuerstenau et al., 1983).Oxidation makes coal surfaces completely hydrophilic(Arnold andAplan,1989)

Bright coals have more vitrinite, less inertinite and mineral than dull coals. Bright surfaces repel water more than dull surfaces because it includes more vitrinite (Shu et al., 2002). Bright coal surfaces have more hydrophobic functional groups than dull coal surfaces, but fewer hydrophilic groups and a lower mineral concentration (Laskowski,2023).The dull coals are primarily composed of inertinite and particles of minerals. In terms of maceral composition, dull coals are more heterogeneous than bright coals. The surface of dull coal is rich in inertinite and mineral particles, making it more hydrophilic. According to Shu et al.(2002) inertinite includes more hydrophilic oxygen-bearing functional groups. XPS examination of bituminous coal by Ding (2009) indicates that the dull surface holds more hydrophilic, oxygen-bearing functional groups, and vitrinite is more hydrophobic compared to inertinite. Although

both coals contain significant mineral matter in the form of quartz, clay, and other aluminosilicates. Singh et al.(2015a) noted that the dull coal has a substantially higher mineral content, and higher Al and Si amounts than the bright sample. The presence of more aliphatic groups in bright coal is indicated by higher resolution C1s spectra, but dull coal should be more hydrophilic due to more oxygen-carrying functional groups, such as carbonyl and carboxyl groups on the surface (Kabe et al., 2014). In terms of surface composition, dull coals are more heterogeneous than bright coals, with more hydrophilic functional groups on their surfaces. The presence of different maceral groups resulted in variances in brightness and hydrophobicity, and vitrinite is brighter and more hydrophobic than inertinite (Fuerstenau et al., 1983; Xia and Zhang, 2017). Hence, it is essential to examine the surface properties of coal, which can be very useful for the coal production, combustion, and environmental point of view. In order to understand these surface properties, XPS and FTIR can be helpful tools. XPS is a surface-sensitive and quantitative survey technique that can analyze chemical bonds on coal at a surface within 10 nm. It is a helpful tool for finding a material's chemical composition, chemical state, and electronic configuration. XPS is also familiar as ESCA (Electron Spectroscopy for Chemical Analysis)(Fu et al., 2018; Liu et al., 2020). In this investigation, XPS was used to decipher the surface features of Indian Permian coal in detail. The surface hydrophobicity of Indian coal was also discussed based on the findings of XPS and FTIR spectroscopic results.

5.6.2. XPS Characterization of the Coal

The results of the ultimate and proximate analysis of volatile bituminous coal sample have been tabulated in Table 5.6. This analysis is carried out to assess general coal characteristics, which helps comprehend the nature and quality of the sample. One gram of each sample was taken for proximate analysis. The loss in weight has

been recorded according to ASTM (American Society for Testing of Standards). It has been noted that the moisture content in the case of IPC-1 is higher as compared to IPC-2. After that, an ultimate analysis was carried out, and it can be seen that carbon content and GCV in the case of IPC-2 were higher than in IPC-1. These values of ultimate analysis have been matched with the XPS results.

Table 5.6 Proximate, ultimate and gross calorific value (GCV)of IPC from the Singrauli coalfield

Samples	Proximate analysis, wt% (ad)				Ultimate analysis, wt% (daf)					GCV kcal/kg
	Moisture	VM	Ash	FC	Carbon	Nitrogen	Hydrogen	Oxygen	sulfur	
IPC-1	5.40	32.60	18.00	44.00	54.84	1.32	4.49	11.53	0.80	5965
IPC-2	4.60	29.50	11.6	54.30	62.00	1.44	4.81	12.50	0.55	6742

The XPS qualitative survey has been carried out to get the information about surface structure and chemical composition and various element or hetero-structures present on the surface of the coal through XPS. For the measurement a spectrum of 0-1350 eV has been collected and resultant spectra shown in the Figure 5.8 and5.9. The spectrum contains various peaks corresponding to C, O, N, S, Si, Cl, Al, As, Fe, Mn, and Cr elements. The high peaks confirm that O and C elements are present in significant composition with corresponding other elements N, S, Si, Cl, Al, As, Fe, Mn, Hg and Cr with low-intensity peaks confirming the minor content of these elements(Fu et al., 2018; Jaiswal and Pal, 2020; Liu et al., 2020; Xia and Zhang, 2017; Zhou et al., 2015).

In the XPS spectra peak of C 1s (286.0 eV), O 1s (534.5 eV), N 1s (399.9 eV), S 2p (158.2 eV), Si 2p (102.7 eV), and Al 2p (75.6 eV) respectively has been fitted through XPS peak fitting software, and the curves have been plotted by using origin software (Origin 2020 student version) given in Figure 5.8 and 5.9(Fu et al., 2018; Grzybek et al., 2002; Liu et al., 2020; Pietrzak et al., 2007; Xia and Niu, 2018; Zhou

et al., 2015).The quantitative analysis of different hetero-atoms present in the XPS spectra has also been carried out using the Gaussian function in origin software. The atomic content of different element concentrations (in atomic %) was estimated by investigating the peak present in XPS wide energy spectrum and tabulated in Table 5.7. The spectra reveal that the atomic content of carbon is 74.22%, and 78.98% oxygen is 16.17%, and 16.38%; nitrogen 1.79 %, and 1.96 %; sulfur is 2.17 %, and 1.08%; aluminum 2.09%, and 2.16%; and silica is 2.52%, and 2.16 %; in IPC-1 and IPC-2 coal samples, respectively.

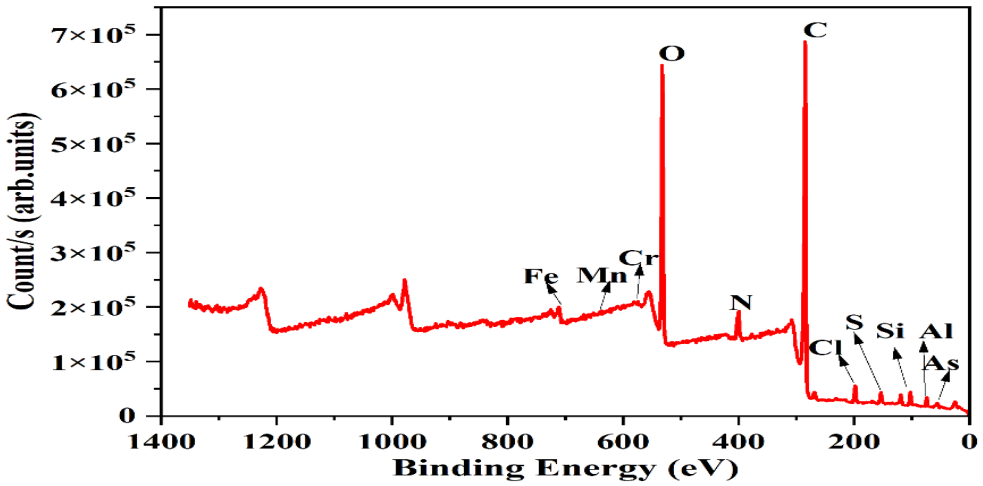

Figure 5.8. XPS wide energy spectrum for the surface of IPC 1coal sample

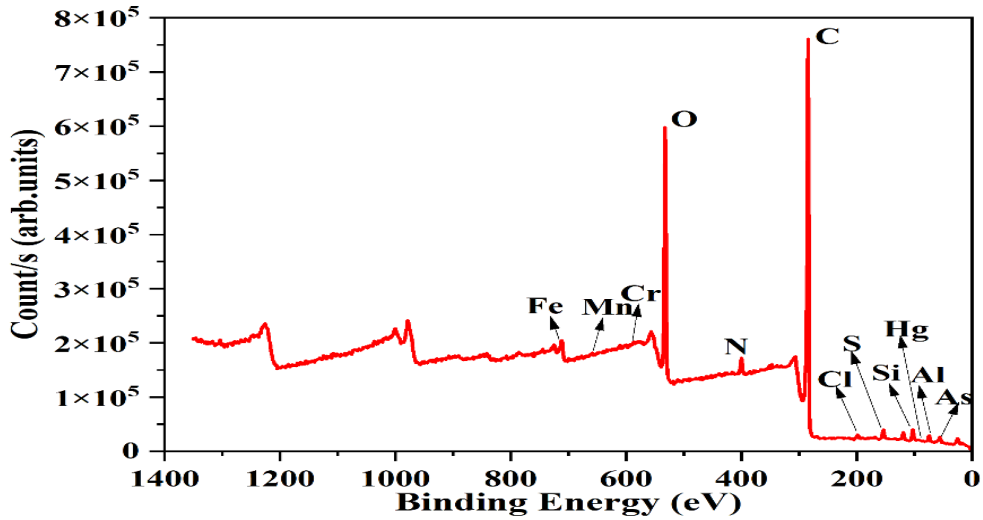

Figure 5.9. XPS wide energy spectrum for the surface of IPC 2 coal sample

Table 5.7 Contents of atomic carbon, atomic oxygen, atomic silica, atomic aluminum, atomic nitrogen, and atomic sulfur on the coal surface.						
Sample ID	C1s (%)	O1s (%)	Si2p (%)	Al2p (%)	N1s (%)	S2p (%)
Binding energy (eV)	286.0	534.5	102.7	75.6	399.9	158.2
IPC -1	74.22	16.17	2.52	2.09	1.79	2.17
IPC -2	78.98	16.38	2.70	2.16	1.96	1.08

Further, it has been observed from the Table 5.7 that the atomic carbon is the main content of the element in the coal samples, and it plays a very significant role on the surface of Indian Permian coal. Carbon as a main organic material might have excellent hydrophobic properties by containing different organic functional groups. From the peak evaluation of carbon (C 1s) given in Figure 5.8 and 5.9, four peaks of binding energy, 284.0 eV, 285.1 eV, 286.6 eV, and 288.5 eV have been obtained correspond to the different forms of carbon, which are C-C or C-H (aromatic graphitized carbon and aliphatic carbon), C-O (alcohol, phenol carbon), C=O (carbonyl or carboxide), or COO- (carboxyl)(Fu et al., 2018; Wang et al., 2017; Xia and Zhang, 2017; Zhang et al., 2018a). The fraction of carbon forms on the surface of Indian Permian coal samples given in Table 5.12

Furthermore, in order to get a better understanding of the C1s spectra, the peak has been fitted and the contents of different species have been evaluated from the deconvolution of the C1s peak, where we get four peaks as shown in Figures 5.12 (a) and 5.13(a) and values are given in Table 5.8.The content of (C-C) aromatic graphitized carbon and (C-H) aliphatic carbon is highest in both IPC-1 and IPC-2, at 67.8% and 70.2%, respectively. Contents of (C-O) alcohol and phenol carbon groups in IPC-1 and IPC-2 are 23.4% and 25.1%, respectively, whereas the amounts of

(C=O) carbonyl or carboxide carbon groups are 4.2% and 3.9% for IPC1 and IPC2 coal samples, respectively. While the content of (COO^-) carboxyl carbon is 1.18% and 0.83% for IPC-1 and IPC-2, which is very small as compared to the other carbon groups. Based on the aforementioned investigations, the total content of aromatic and aliphatic carbons (C-C and C-H) is much higher than the other carbon groups, such as C-O, C=O, and COO^-. As we know, C-O, C=O, and COO^-groups are hydrophilic in nature, while C-C and C-H groups are hydrophobic in nature(Xia and Zhang, 2017). Hence, it can be said that Indian Permian coal has a high ratio of hydrophobic carbon groups as compared to hydrophilic carbon groups. So, the natural hydrophobicity of the Indian Permian coal sample might be high.

Table 5.8 XPS data of C 1s spectra of Indian Permian coal samples IPC-1 and IPC-2

S.N.	Binding energy (eV)	Form of carbon	Content (mol %)	
			IPC 1	IPC 2
1.	284.0	(C-C) and (C-H) aromatic graphitized carbon and aliphatic carbon	67.80	70.30
2.	285.1	(C-O)alcohol, phenol carbon	23.40	25.10
3.	286.6	(COO^-)carboxyl carbon	1.18	0.83
4.	288.5	(C=O)carbonyl or carboxide carbon	4.20	3.90

The constituent estimation of O 1s peak has been carried out, and the corresponding deconvolution gives three peaks as represented in Figures 5.10(b) and5.11(b).The values of binding energy and constituent percentage of groups have been given in Table 5.9. It can be observed that the fitting of O 1s peak gives three binding energies, 531.5, 532.7, and 533.9, corresponding to carbonyl or carboxide carbon, (C-O) alcohol, phenol carbon, and (COO-) carboxyl carbon groups, respectively (Wang et al., 2017; Xia and Zhang, 2017; Zhou et al., 2015). The percentages of these groups in IPC-1, and IPC-2 are 65.2%, 57.1% for (C=O), 21.6%,

38.1% for (C-O), and 3.7%, 1.9% for (COO-), respectively.

Table 5.9 XPS data of O 1s spectra of Indian Permian coal samples IPC-1 and IPC-2

S.N.	Binding energy (eV)	Form of oxygen	Content (mol %)	
			IPC 1	IPC 2
1.	531.5	C=O carbonyl or carboxide carbon	65.2	57.1
2.	532.7	(C-O)alcohol, phenol carbon	21.6	38.1
3.	533.9	(COO^-)carboxyl carbon	3.7	1.9

Further, the constituent estimation of N 1s spectra also gives four peaks displayed in Figures 5.12(c) and 5.13(c) for IPC-1 and IPC-2. These peaks correspond to different nitrogen groups: Pyridine nitrogen, pyrrolic nitrogen, quaternary, and oxidized nitrogen with the binding energy of 398.2eV, 399.4eV, 400.4eV, and 401.8eV, respectively, in both the coal samples given in Table 5.14 (Fu et al., 2018; Jaiswal and Pal, 2020; Liu et al., 2020). The percentage compositions of these groups in IPC 1 and IPC 2 are pyridine nitrogen 17.10 % and 11.6%,respectively,pyrrolic nitrogen 48.3%, 51.70% quaternary 6.41%, 4.21%, and oxidized nitrogen 11.80%, 10.20%, and 11.70%, respectively.

Table 5.10 XPS data of N 1s spectra of Indian Permian coal type samples IPC 1 and IPC 2

S.N.	Binding energy (eV)	Form of Nitrogen	Content (mol %)	
			IPC 1	IPC 2
1.	398.2	Pyridine nitrogen	17.10	11.60
2.	399.4	Pyrrolic nitrogen	48.30	51.70
3.	400.4	Quaternary nitrogen	6.41	4.21
4.	401.8	Oxidized nitrogen	11.80	10.20

Furthermore, the XPS peak contains Si 2p peak and Al 2p peaks at 102.7 eV and 75.6 eV, respectively, which specify the presence of Si 2p and Al 2p in Indian Permian coal samples IPC 1 and IPC 2, respectively (Liu et al., 2020; Xia and Zhang,

2017).

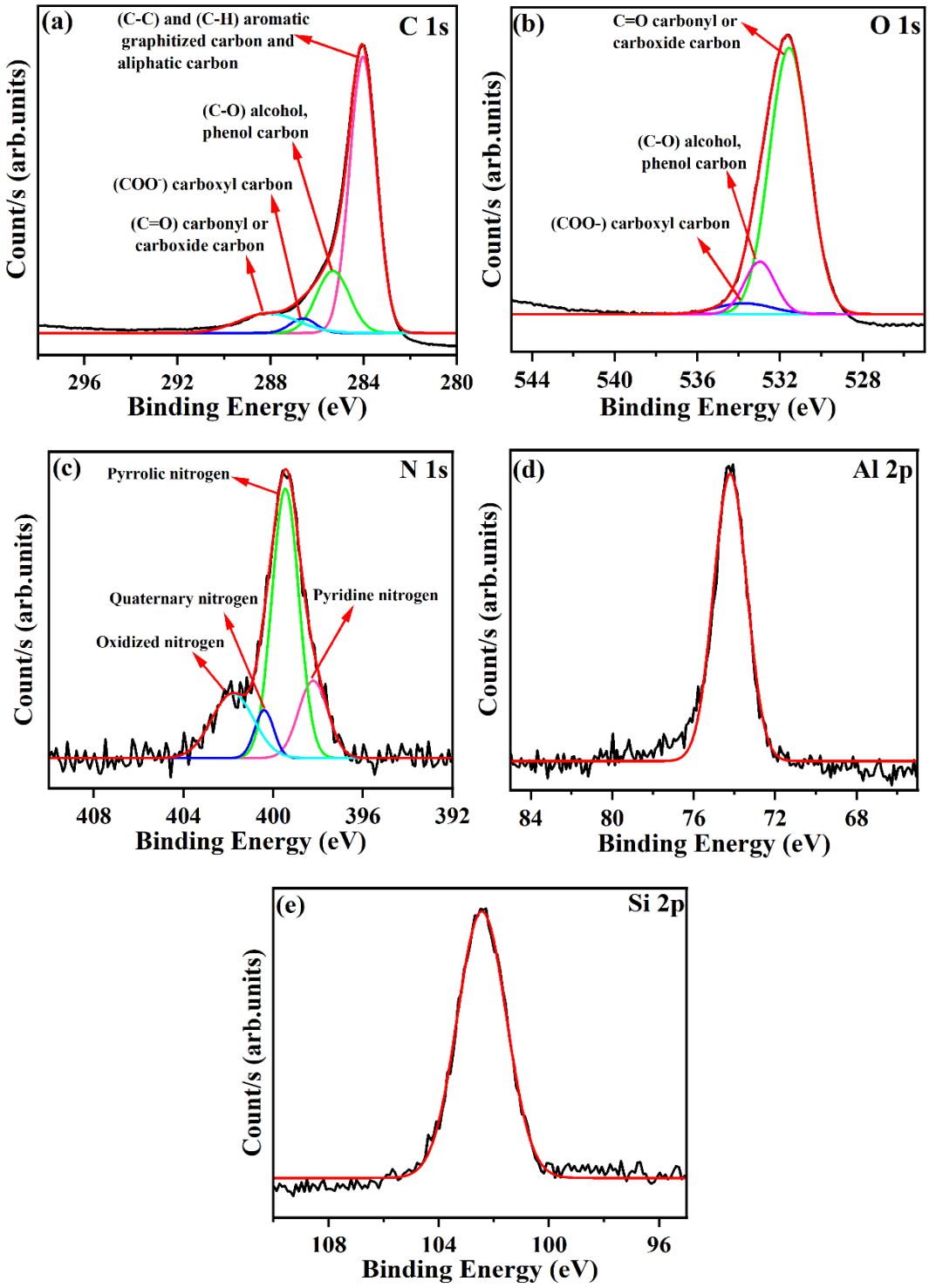

Figure 5.10. XPS spectra of coal sample IPC1 for **(a)** C1s peak, **(b)** O 1s peak, **(c)** N 1s peak, **(d)** Al 2p peak, and **(e)** Si 2p peak, black solid line and red solid line refer to experimental curves and best-fitted curves, and the assignment of peak is also given after deconvolutions with a solid line of different colour.

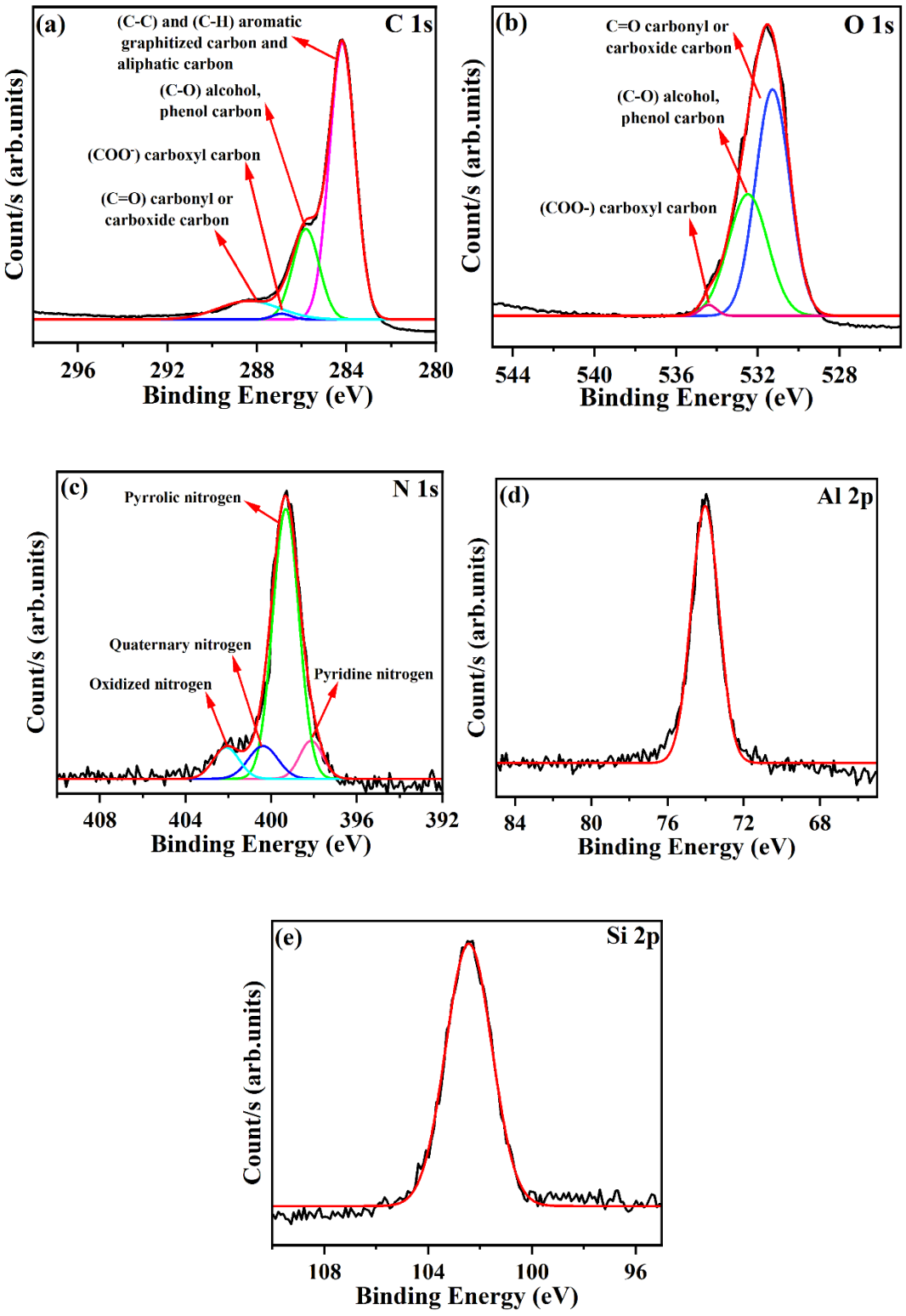

Figure 5.11. XPS spectra of coal sample IPC 2 for **(a)** C1s peak, **(b)** O 1s peak, **(c)** N 1s peak**, (d)** Al 2p peak, and (e) Si 2p peak, black solid line and red solid line refer to experimental curves and best-fitted curves, and the assignment of peak is also given after deconvolution with a solid line of different color.

In Figures 5.10 and 5.11(d) and (e) represent the fitted specters of Al 2p and Si 2p, respectively. It can be seen from Figures 5.10 and 5.11(d) and (e) that the fitting is perfect and corresponds to the Al_2O_3(clay groups) in the case of Al 2p and quartz in the case of Si 2p spectra.

5.6.3 Conclusion: The XPS survey spectrums confirm the presence of different elements on the surface of the coal. Some of these are C 1s (286.0 eV), O 1s (534.5 eV), N 1s (399.9 eV), S 2p (158.2 eV), such as SiO_2 and Al_2O_3 which correspond to Si 2p (102.7 eV) and Al 2p (75.6 eV) with quartz and clay group minerals on the surface of coal. XPS spectra of C 1s confirm a huge amount of aliphatic and aromatic carbon present, which are hydrophobic compared to hydrophilic groups such as alcoholic carboxylic and phenolic groups.

5.7 Raman Spectroscopic Analysis

5.7.1 Introduction: Raman spectroscopy is a simple; fast; precise; and a repeatable, non-destructible quantitative and qualitative tool that can be used for examining various samples containing organic carbonaceous materials. Different thermochemical properties of coal can be analyzed with the help of this technique (Quirico et al., 2005). The Raman spectrum can provide geologically relevant information by avoiding or decreasing analytical biases, and it can be used as a versatile technique for the identification and characterization of graphitic carbons in geological and environmental materials (Speight, 2016). Raman spectroscopy is used in conjunction with infrared absorption spectroscopy. Both probe vibrations within a compound, but their selection rules differ. In basic circumstances, molecular geometry can be determined by analyzing multiple peaks that are present or absent in the two spectra of a molecule (Roy et al., 2021; Thankan et al., 2023).This technique helps in

studying the chemical structure, quality, and nature of organic matter, as well as the facts that catalyze the chemical process and heavy fraction leaching process, as well as the organic matter maturity, chemical structure, and thermal maturity of organic carbon present in coal-related to coal utilization (Cheng et al., 2022).

5.7.2 Raman characterization of the coals

Figure 5.12 represents the Raman spectra of the four medium volatile bituminous coal samples for the range of 1000-2000 cm^{-1}. It is seen from the Raman spectra from Figure 5.12 that there are two prominent Raman vibrational frequency bands located nearer 1370 cm^{-1}, reorganized as the D band (deformation band), and the band near 1590 cm^{-1} represented as the G (graphitic band) band. The D band peaks arise due to Raman activity of A1g symmetry, which have been associated with lattice defects, discontinuity, and irregular hexagonal lattice structure of the Sp2 network of carbon present in coal and the G band arises by C stretching of double bounded aromatic rings (Jiang et al., 2019; Li et al., 2021; Nestler et al., 2003; Xie et al., 2019; Yin et al., 2019).

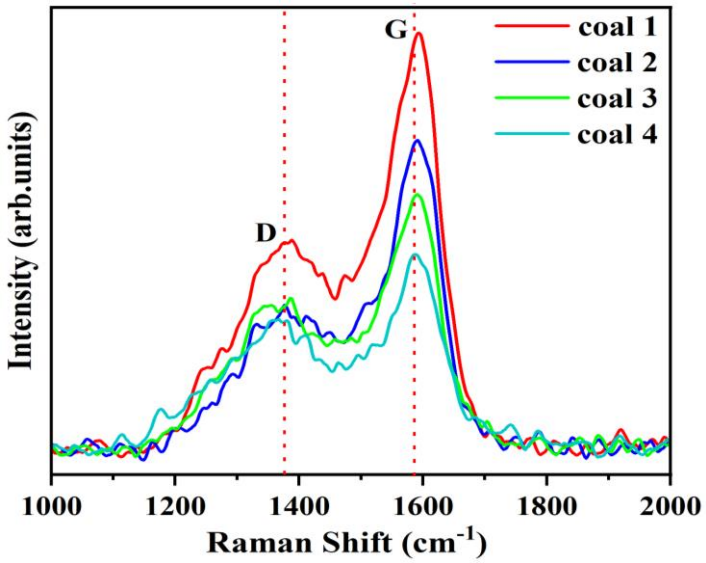

Figure 5.12. Raman spectra of coal 1-4 for different band

These vibrations are related to the molecular structures and identifiable vibration of the aromatic E2g2 plane. The peak intensity of the D bands are smaller than that of the G band, and there are also D and G bands overlapped. The study of only D and G bands to understand the Raman spectra of coal is not enough and results in the loss of information about the properties of the collected coal samples (Hinrichs et al., 2014; Jiang et al., 2019; Jiang et al., 2021; Xie et al., 2019). Hence, integrating Raman spectra of coal by the curve fitting and smoothing method is essential to investigate and obtain the hidden valuable information in the overlapped Raman coal spectra. Therefore, Raman peaks are further deconvoluted in origin software using the Lorentz function and further used to determine and discuss the position of peaks, coal properties, and other information from the deconvoluted peaks obtained from overlapped peaks. We found that the D and G band peaks were the most prominent and deconvoluted into five different peaks; four of them are Lorentz peaks (D_1, D_2, D_4, and G) located near 1137 cm^{-1}, 1610 cm^{-1}, 1240 cm^{-1}, and 1585 cm^{-1} respectively, and one Gaussian peak (D_3) near 1500 cm^{-1}. The five peaks obtained by deconvolution have been represented in Figure 5.13 (a-d). Various carbonaceous structures accompany these peaks**.** The five bands obtained are as follows: D_1 band near 1370 cm^{-1} corresponds to a defect in the graphite structure of coal; D_2 band linear at 1610 cm^{-1} conforms to defects at the edges of the graphite planes type structure; D_3 band near 1500 cm^{-1} confirms the amorphous phase of coal; D_4 peak near 1240 cm^{-1} confirms the extended carbon chains present in coal; and the G peak near 1585 cm^{-1} corresponds to the graphite phase of coal (He et al., 2017; Malysheva et al., 2020; Sonibare et al., 2010). It is well known that the position of G and D_1 peaks, the difference in the peak positions of D_1 and G peaks, and the ratio of integrated areas of the peaks are important parameters to estimate the degree of crystalline defect in

carbonaceous collected samples. Hence, the band position, difference of G-$D_1$and the ratio of peak area AD_1/AG, AD_1/A_{All}, and AG/A_{All} obtained in deconvolution are also tabulated in Table 5.11.

Table 5.11 shows that the positions of D_1 and G peaks in all the four coal samples are closer to each other and located nearer 1370 $cm^{-1}$and 1590 cm^{-1}, respectively. This means the structural order in all four-coal samples is approximately the same. The G and D_1 peak range is between 208 and 230 cm^{-1}. The value of the G-D1 peak in coal 1 is higher, and peak positions are also the largest compared to the other three samples, indicating that coal 1 has a less distorted structure than the other coal samples. The integrated area A_{D1}/A_G ratio gives information about the degree of order of structure, and the lower ratio value of A_{D1}/A_G signifies the higher-ordered structure. The ratio of A_{D1}/A_G also represents the degree of growth of aromatic rings in coal, and decreases in the ratio of A_{D1}/A_G represent the growth of aromatic rings, which means the developed structure is closer to the graphite structure (He et al., 2017; Jiang et al., 2019; Sheng, 2007; Zhu et al., 2017). Table 5.11 shows that the ratio of integrated peak area, i.e., I_{D1}/I_G, is 0.388 to 0.963 for all the coal samples. For coal, 4, the ratio of I_{D1}/I_G is highest (0.963), which indicates the degree of graphitization, is lowest. Coal 1 has a lower ratio value of I_{D1}/I_G (0.388), signifying a well-graphitized coal structure. The ratio of the area of A_{D2}/A_{All} gives information about the relative concentration of amorphous carbon present in the coal; a decrease in the ratio of A_{D2}/A_{All} indicates a decrease in the amorphous nature of coal and an increase in the order of coal molecule structure (Jiang et al., 2019; Sonibare et al., 2010; Zhu et al., 2017). The value of $A_{D2}/A_{All}$is smaller (0.157) for coal 1, over the coal 2,coal 3, and coal 4; hence coal 4 has a more ordered structure and is less amorphous.

Table 5.11 Raman structural parameters determined from the fitting of Raman spectrum									
Coal Sample	**Position (cm^{-1})**						**Ratio of Peak Areas**		
	D_4	D_1	D_3	G	D_2	G-D_1	A_{D1}/A_G	A_{D2}/A_{All}	A_G/A_{All}
Coal 1	1248	1365	1475	1582	1605	230	0.388	0.157	0.406
Coal 2	1233	1368	1510	1592	1610	208	0.875	0.347	0.396
Coal 3	1247	1374	1506	1592	1602	225	0.889	0.401	0.450
Coal 4	1246	1379	1498	1585	1608	213	0.963	0.432	0.448

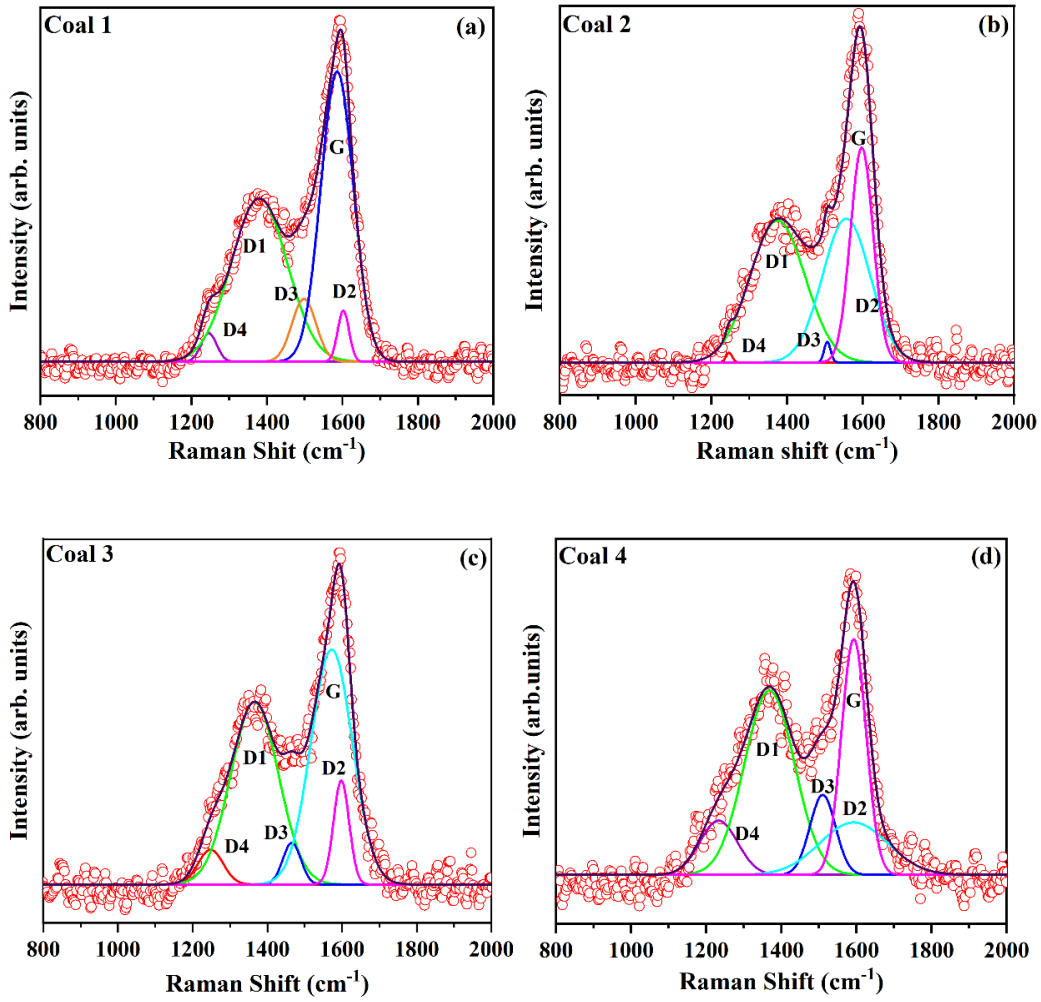

Figure 5.13 (a-d). Raman spectrum of four different samples coal with the corresponding curve fitted bands (red dotted represents experimental Raman spectra; black line fitting spectra, different color line represent area under D1, D2, D3, D4, and G)

5.7.3 Conclusion: Raman spectral methods are powerful tools for the non-destructive qualitative and semi-quantitative analysis of coal. Raman spectra in 1000 to 2000 cm^{-1} range were obtained, revealing two prominent peaks in coal known as the D and G bands, which were located near 1370 cm^{-1} and 1590 cm^{-1}, respectively. G-D1 value for coal 1 was 230, indicating less distorted graphitic structures. The ratio of A_{D1}/A_G represents the degree of growth of aromatic rings in coal, indicating that coal 1 has a less distorted structure than the other. The value of A_{D2}/A_{All} was smaller (0.157) for coal 1 than the coal 2, coal 3, and coal 4; hence coal 4 has a more ordered structure and was less amorphous. The A_{D1}/A_G ratio of 0.388 indicates a higher order structure. For Coal 4 A_{D1}/A_G ratio of 0.963 indicates less ordered structure. The samples' G-D1, ID1/IG ranged from 208 to 230 cm^{-1}, 0.388 to 0.963, respectively. For coal 4, the ratio of I_{D1}/I_G was highest (0.963), which indicates the degree of graphitization was lowest. Coal 1 has a lower ratio value of I_{D1}/I_G (0.388), which signifies a well-graphitized coal structure. The I_D/I_G ratio decrease indicates that graphitization has increased in coal. A decrease in the ratio of A_{D2}/A_{All} indicates a reduction in the amorphous nature of coal and an increase in the order of coal molecular structure. The value of A_{D2}/A_{All} was smaller (0.157) for coal 1 than (0.347) for coal 2. Hence, coal 4 has a more ordered structure and is less amorphous.

5.8 Characterization Coal-derived fly ash

5.8.1 Introduction: Fly ash (FA) is a fine, powdery residue produced by coal combustion that is transported from the firebox through the boiler by flue gases (Hower et al., 2017c). In this study, fly ash samples were collected from the thermal power plant that supplies coal from the Jayant collieries located in the Singrauli coalfield. Coal combustion generates a considerable amount of fly ash, and its management is a huge problem (Dwivedi et al., 2014). General characteristics

(geochemical and mineralogical) of coal fly ash have been carried out to assess its chemical nature and behavior using SEM-EDX and XRF. Table 5.12 shows the amounts of various oxides in Permian coal-derived fly ash samples coded as PFA1, PFA2, PFA3, and PFA4, respectively. Fly ash morphological and chemical properties like morphological features, elements, oxide concentration, and toxicity have been discussed because fly ash is a byproduct of coal and has serious environmental consequences. A thorough understanding of its chemical properties is required for its application and utilization (Silva et al., 2010). In this study, the fly ash chemistry was also correlated with coal chemistry, which is essential to understanding the environmental risk associated with contamination of the surrounding region. The nanoparticles related to fly ash form an aggregate containing amorphous hazardous heavy metals and elements (Silva et al., 2012). For their investigation, medium-volatile bituminous coal from a single mine was burned in order to study the connection between the coal geochemistry and the FA chemistry.

5.8.2 Morphological Features

Generally, FA particles are spherical and have different size distributions. FA typically has a high surface area and is light in texture because of the presence of large porous and carbonaceous particles along with glass (Saikia et al., 2021b). Fly ash has a low bulk density, and its water holding capacity ranges from 49 to 66% on a weight basis (Kumar et al., 2015b). In SEM images, different morphological shapes of FA have been observed as amorphous, non-opaque, rounded, vesicular-angular, and carrying cenospheres of different sizes. The surface morphology of the cenospheres depends on the exposure time to combustion and other temperature conditions (Ranjbar and Kuenzel, 2017). Agglomeration of large particles has been observed, and many spherical particles, together with irregular-shaped particles, have formed

amorphous patterns in PFA. The colour of fly ash depends on the iron oxide concentrations and unburned carbon present in the sample. FA is commonly found in white, deep red, brown, white, or yellow-white colour (Kumar et al. 2015).

The cooling rate of FA particles affects the composition of inorganic matter formation. Fast cooling results in the formation of small glassy particles, while slow cooling results in the formation of large crystalline particles (Alterary and Marei, 2021).Most of the particles in the fly ash samples were observed to have irregular shapes, which could be attributed to the fact that even at a temperature of 800 ˚C, the particles didn't undergo melting but instead softened and formed irregular shapes (Seo et al., 2010). The irregular-shaped components were formed during combustion as a result of unburnt carbon as well as the secondary creation of anhydrite and calcite (Gopinathan et al., 2022). Zanjad et al. (2022) noted irregular shapes because some minerals like hematite do not melt but distort in shape at temperatures above 800^{o}C. Associated minerals, especially silica in coal, were melted in the glass during coal combustion, and liquid droplets of fine to ultrafine particles were emitted with other gases (Aughenbaugh et al., 2016). Rapid coalescence of these gases resulted in their conversion into glass particles.Glass is composed of silica, and unburned carbon and residual carbon material are associated with nano minerals (Martinello et al., 2014).

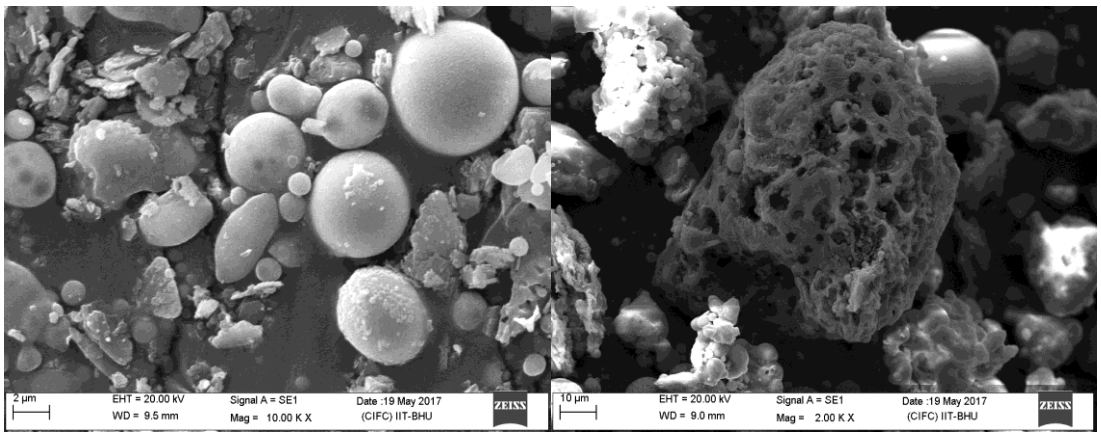

Figure 5.14: SEM image showing agglomerated glass, cenospheres and nanosphere.

5.8.3 Basic Chemistry and Elements

The fly ash was investigated using XRF, and a scanning electron microscope with energy dispersive X-ray spectroscopy (SEM-EDX). SEM is utilized to identify FA amorphous phase composition, and the EDX survey is used to identify the elemental composition. SEM is helpful to identify the pattern of flexure and the cracks in the specimen (Kutchko and Kim, 2006). The Permian coal in Jayant mine is amedium-volatile bituminous coal and is characterized by high contents of moisture (7.1%), volatile matter (28.9%), and ash (19.46%). Fly ash is mostly composed of silica, aluminium, iron, calcium, and oxygen elements. The inorganic matter consisting of amorphous and crystalline phases represents the bulk composition of FA. The nanoparticles present in coal fly ash form aggregates containing amorphous hazardous elements. The major elements in the fly ash samples, as determined by EDS, were silicon, aluminum, iron, calcium, and oxygen in different compounds. Aluminium was primarily associated with silicon (Saikia et al., 2014b). The relatively weak signal intensities for sodium, potassium, magnesium, calcium, and iron indicate lower concentrations of these elements in the fly ash.

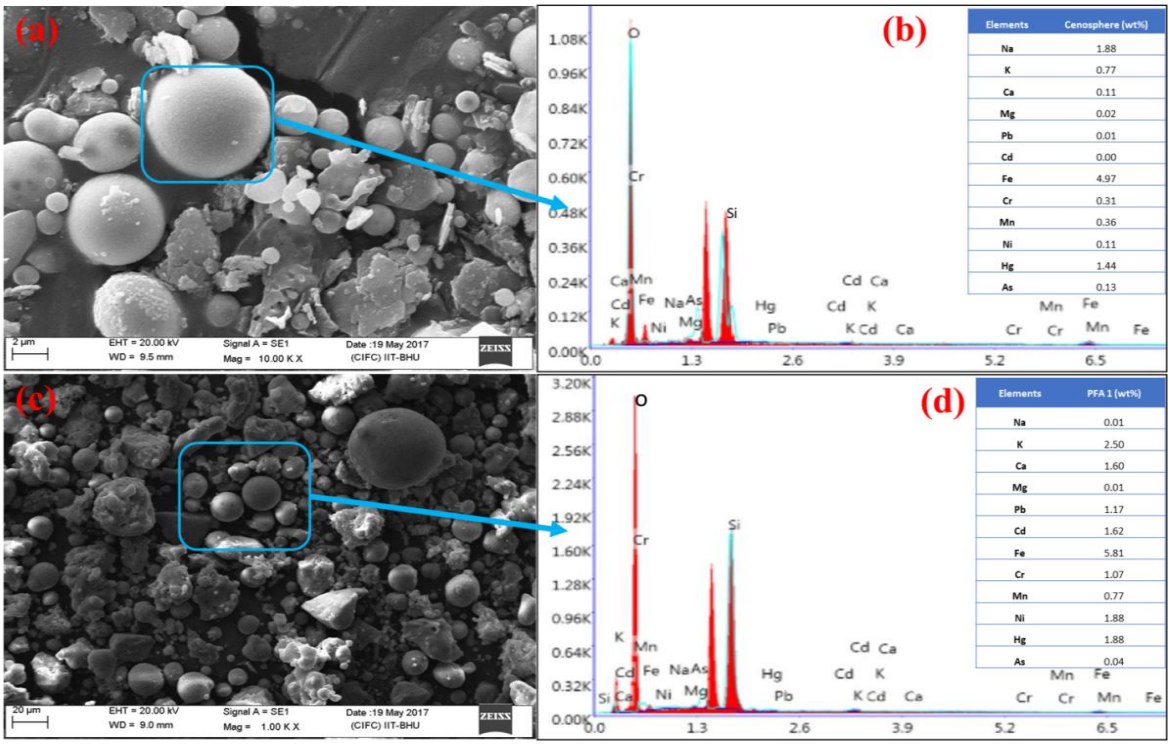

Figure 5.15: Energy-dispersive X-ray spectroscopy (EDX) graph of elements associated with the Permian fly ash. The survey detected the presence of carbon, oxygen, silicon, and aluminum as significant constituents.

Figure 5.15 shows the SEM images and EDX patterns of fly ash. As shown, the spherical shape in general and morphology of each FA particle were significantly varied because of their complex formation process in coal combustion. The concentration of trace elements in the FA is strongly related to the concentration of elements in the feed coal. Inefficient combustion of coal indicates the presence of unburned carbon in fly ash (Hower et al., 2000). The nature and characteristics of unburned carbon depend on the rank and type of feed coal and combustion conditions (Hower et al., 2017b).The inertinite group of macerals is inherently more difficult to combust than the associated vitrinite group. Hower et al. (2017b) observed that the thermal degradation of sulphides and iron-containing minerals led to the generation of magnetite and other spinal varieties containing nickel, chromium, and aluminum. The primary drivers of FA chemistry are the type of coal burned, the cooling temperature

and control devices used, and other combustion specifications(Gupta et al., 2019b).

The major oxides in fly ash samples were SiO_2, Al_2O_3, CaO, MgO, MnO, Na_2O, K_2O, and Fe_2O_3. The oxide chemistry of fly ash is presented in Table 5.12. FA was primarily made up of iron, calcium, alumina, and silica oxides. The composition by weight of the total fly ash produced after combustion depends on the percentage of mineral matter present, especially ash content in coal, the pulverized size of coal, and the temperature condition of boilers (Ward, 2016b). Combustor fly ash accounts for nearly 70% of the solid waste generated by power plants (Dwivedi et al., 2014). As CaO increases in PFA 1, SiO_2/Al_2O_3 decreases. The percentage of SiO_2 in fly ash varies from 46.50 to 50.70wt%, with the highest value observed in PFA 3 (50.70%). The presence of silica is an essential aspect of accessing the pozzolanic potential of fly ash. The pozzolanic activity of FA helps densify concrete-based products and is responsible for the reaction between fly ash and lime in compressed FA bricks (Nayak et al., 2022).

The percentage of alumina in fly ash varies from 28.30 to 23.60 wt%, with the highest value observed in PFA 3 (28.30 wt%). PFA 4 shows the highest SiO_2/Al_2O_3 ratio (2.03% wt%). Alumina (Al_20_3) is beneficial for concrete and fly ash-based cement by providing strength(Singh and Subramaniam, 2018). Calcium oxide (CaO) is present at its highest level in PFA1 (10.40 wt%) because the feed coal is rich in calcium-rich alumino-silicates. Based on Calcium oxide (CaO) percentage, a low level of calcium in feed coal creates alumino-silicate glass, while a high calcium content results in the formation of calcium alumino-silicate glass (Goodarzi, 2006). Ca-bearing phases in the ash may include alumino-silicates, oxides, hydroxides, carbonates, sulphides, and sulphates. It is well recognized that, compared with high-rank coals, low-rank coals are generally richer in Ca and Mg (Fan et al., 2019).

Sodium oxide (Na_2O) and potassium oxide (K_2O), also known as alkali oxides, are present in smaller proportions.

Table 5.12.The concentration of major oxides (wt%) of PFA from the Singrauli coalfield.

Oxides	**PFA 1**	**PFA 2**	**PFA 3**	**PFA 4**	**Mean value**
SiO_2	48.90	46.50	50.70	48.20	48.57
Al_2O_3	27.70	23.60	28.30	23.70	25.82
CaO	10.40	9.10	7.20	7.90	8.65
Fe_2O_3	3.20	8.10	8.30	10.40	7.50
MgO	4.90	3.50	0.70	0.80	2.40
MnO	2.60	4.90	2.10	4.50	3.52
Na_2 O	1.90	2.70	1.50	2.90	2.25
K_2O	0.40	1.60	1.20	1.60	1.20
SiO_2/ Al_2 O_3	1.76	1.97	1.79	2.03	1.88

As seen in Table 5.12**,** potassium oxides are present in all samples and range from 1.60 to 0.40 wt%. The higher percentage of alkali can lead to an alkaline reaction and delay the hydration activity (Wilińska et al., 2018). Thus, the nature of fly ash samples was found to be primarily alkaline. FA was mostly composed of iron, calcium, alumina, and silica. The oxides chemistry differs in different FAs due to differences in the source and combustion conditions (Hower et al., 2022b).

It is obvious from the collected data that silicon dioxide (Quartz-SiO_2) is the most abundant element, followed by aluminium, calcium, and iron oxides (Si > Al > Ca > Fe). The fly ash obtained from thermal power plants has silica as a dominant component, and glass is composed of silica glass (Saikia et al., 2021b). Gopinathan et

al., (2022) noted that Permian coal fly ash is non-toxic at lower concentrations, whereas at higher concentrations, the same may be toxic to the environment. Prolonged exposure to aromatic organic chemicals found in coal-derived gases would be hazardous to health. The nanoparticles observed in Permian fly ash form an aggregate containing various amorphous hazardous elements. The greater surface areas of ultrafine fly ash as compared with larger particles with the same chemistry make them more environmentally active towards bio-uptake and associated health risks. SEM-EDX surveys show the presence of mercury in fly ash samples. Hower et al. (2009b) reported that mercury discharging from typical flue gas generally existed in three forms, i.e., elemental mercury (Hg^0), oxidized mercury (Hg^{2+}) and particulate bound mercury (Hg^p).The presence of mercury indicates that anisotropic coke, having a large surface area, appears to adsorb mercury from the flue gas stream. Hg adsorption generally increases with density and surface area (Hower et al., 2000). Aggregation of fly ash in large quantities and the presence of toxic elements in higher concentrations will cause severe environmental and health hazards, and the dumping of fly ash in landfills and slurry ponds has the potential to contaminate water and soil resources (Kanchan et al., 2015).Smaller fly ash particles (less than 2.5 µm) can easily escape into the atmosphere. Upon prolonged inhalation, these particles penetrate deep into the body and settle in the lungs, which eventually causes cardiovascular disorders, cerebrovascular diseases, and even lung cancer (Reynolds et al., 2003). Hower et al., (2009b) observed and measured the level of mercury and other hazardous gases from coal-fire gas vents and the variety of harmful organic compounds released into the atmosphere. Mercury and arsenic are volatile elements that can be released into the atmosphere very easily. Mercury is considered the most hazardous and toxic heavy metal, emitted almost totally in vapour form into the

environment (Hower et al., 2010). Hower et al. (2009a) noticed that coal-fire vents have been emitting different types of volatile organic compounds, mercury, and other dangerous pollutants, along with sulphur compounds. Organic chemicals like benzene are dangerous and carcinogenic. People who live close to a power station may suffer severe health effects if they are exposed to the fumes released from coal burning for an extended period of time.

The trace element concentration in the FA is strongly related to the concentration of elements present in the feed coal. More volatile heavy metals such as lead, zinc, and cadmium would tend to vaporize and recondense on fine particles (Mardon and Hower, 2004). The elements As, Cd, Cr, Cu, Mo, Ni, Pb, Zn,Hg, Cl, and F are of potential environmental concern. The trace element concentrations in FA are sometimes 4–10 times higher than those in the parent coal (Yao et al., 2015). Generally, the chemical properties of FA are influenced to a large extent by the properties of the coal burned and the techniques used for the handling and storage of coal. The combination of decreasing temperatures and increasing surface areas of FA particles leads to enhanced concentrations of volatile trace elements. Indian Permian coals are allochthonous in origin, so the principal elemental makeup of coal ash is comparable to the content of a wide variety of rocks found in the upper lithosphere since ash is generated from inorganic minerals found in coal, including quartz, feldspars, clays, and metal oxides (Chandra and Chakrabarti, 1989; Zierold and Odoh, 2020). Finkelman et al., (1990) investigated the leaching behavior of elements in coal of different ranks. He found that low-rank coals were generally richer in exchangeable Ca and Mg than high-rank coals (Finkelman et al., 2021b). In lower-rank coal, mineral matter is present as dissolved salt in pore water, attached to organic compounds and other crystalline and non-crystalline inorganic compounds (Hower

and Robertson, 2004). At high temperatures, the metamorphic changes of coal-associated inorganics are responsible for the generation of different oxide phases. Fly ash utilization is based on its chemical properties; thus, identification of the causes and distribution of those properties in fly ash is essential. The presence of silica and silica-alumina-based materials in FA provides pozzolanic properties, and its incorporation in concrete is a partial substitution for cement. The cenospheres with high alumina content have good mechanical strength (McCarthy et al., 2019).

5.8.4 Conclusion

To know the structural features, basic chemistry, and elements present in Permian FA, SEM-EDX, and XRF techniques were used. Coal undergoes remarkable morphological changes with minerals and other inorganic portions during combustion. The presence of highly aggregated crystalline glass was found in fly ash. Chiefly, silica and alumina-based compounds are dominant, along with iron and calcium oxides. SEM-EDX shows the presence of potentially dangerous elements (Pb, Cd, Fe, Cr, Mn, Ni, Hg, and As) in the PFA. The XRF study indicates the presence of major oxides (SiO_2, Al_2O_3, Fe_2O_3, and CaO) in fly ash. However, further research is required to comprehend the toxicological relationships between the physicochemical and morphological features of coal and fly ash, which contribute to the environmental and human health implications near coal-based thermal power plants. Because the use of fly ash is based on its chemical attributes, it is important to identify the sources and distribution of those properties in fly ash. The chemical composition of coal fly ash varies depending on the geochemical properties of the coal being burned.